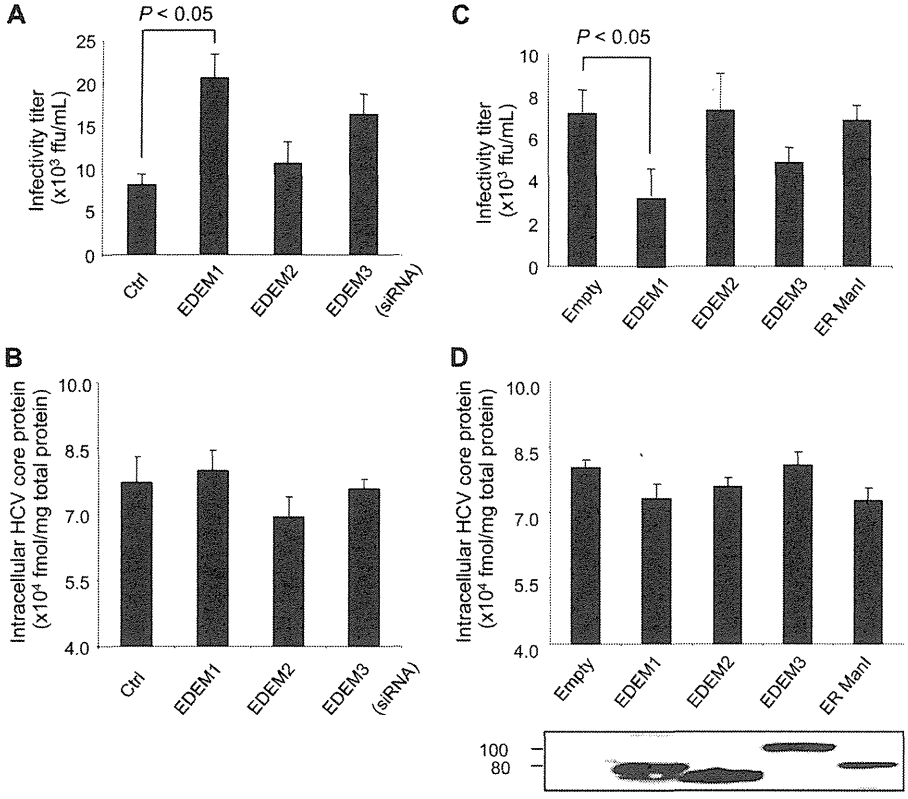

FIGURE 4. **Role of EDEMs in HCV replication and production of infectious virus particles.** *A*, HCV production in HuH-7 cells transfected with EDEM siRNAs. Cells were infected with JFH-1 at a m.o.i. of 1. Twenty-four hours later, the cells were transfected with the indicated siRNAs at a final concentration of 10 nM. The culture medium was harvested 48 h later and was used to infect naïve HuH-7.5.1 cells seeded in a 96-well plate. Immunostaining using anti-HCV core antibodies was performed at 72 h after infection, and focus-forming units were counted. *B*, siRNA-transfected and HCV-infected cells described in *A* harvested at 48 h after infection. Intracellular HCV core protein was measured. The values were normalized to total protein in the cell lysate samples. *C*, HCV production in HuH-7 cells transfected with plasmids carrying EDEM1-HA, EDEM2-HA, EDEM3-HA, or ER ManI-HA genes. *D*, intracellular HCV core protein within the cells described in *C*. Expression levels of the EDEMs and ER ManI were determined by anti-HA immunoblotting. The mean ± S.D. (*error bars*) of three independent experiments are shown in all of the *panels*.

Chemical Inhibition of the ERAD Pathway Increases HCV Production—KIF, a potent inhibitor of ER mannosidase, is reported to inhibit the ERAD pathway. When HCV-infected cells were treated with KIF, virus production increased in the culture medium in a dose-dependent manner (Fig. 5*A*, *left*), and the steady-state level of E2 in the cells increased accordingly (Fig. 5*A*, *right*). No change was observed in intracellular HCV core protein levels after KIF treatment (Fig. 5*A*, *center*). Kinetic analyses showed that E2 was stabilized dramatically in KIF-treated cells (Fig. 5*B*), whereas the fate of HCV core protein, a nonglycoprotein, was not affected by KIF treatment (supplemental Fig. S5). No effect on virus replication was observed when the cells harboring JFH-1 subgenomic replicons were treated with KIF (data not shown).

On the basis of these findings, one may hypothesize that KIF contributes to the stabilization of HCV glycoprotein(s) by interfering with the interaction between (i) EDEMs and viral proteins, or (ii) EDEMs and SEL1L. To address this, HCV E2 was co-expressed in 293T cells with EDEM1, EDEM2, EDEM3, or ER ManI in the presence or absence of KIF, followed by immunoprecipitation (Fig. 5*C*). E2 was shown to interact with EDEM1, EDEM2, and EDEM3, analogous to the data shown in Fig. 3*A*, and KIF did not block the interactions. Decreased electrophoretic mobility of E2 was detected in KIF-treated cells, possibly due to a change in glycan composition caused by inhibition of mannosidase activity. These findings led us to investigate whether the glycans on HCV glycoproteins are required for binding to EDEMs. We generated E1 and E2 mutants by replacing their *N*-glycosylation sites with glutamine residues and analyzed their interaction with EDEMs. Removal of the glycans did not inhibit the binding of E1 and E2 proteins to EDEM, demonstrating that *N*-glycans on the surface of viral proteins are not indispensible for an interaction between EDEMs and HCV glycoproteins to occur (supplemental Fig. S6). The effect of KIF on the association of EDEMs with downstream ERAD machinery was examined further. In cells co-expressing E2 and EDEMs, the interaction of SEL1L with EDEM1 and EDEM3 was significantly reduced in the presence of KIF ($p < 0.05$) (Fig. 5*C*). Consistent with these results, KIF abrogated the EDEM1- and EDEM3-mediated ubiquitylation of HCV E2 protein (Fig. 5*D*). This inhibitory effect of KIF on the SEL1L-EDEM interaction was also observed in HuH-7 cells (supplemental Fig. S7). These results suggest that KIF stabilizes HCV glycoproteins by interfering with the SEL1L-EDEM interaction and thus leads to an increase in virus production.

Role of ERAD in the Life Cycle of JEV—This study demonstrates involvement of the ERAD pathway in HCV production. However, the role of this pathway in the production of other

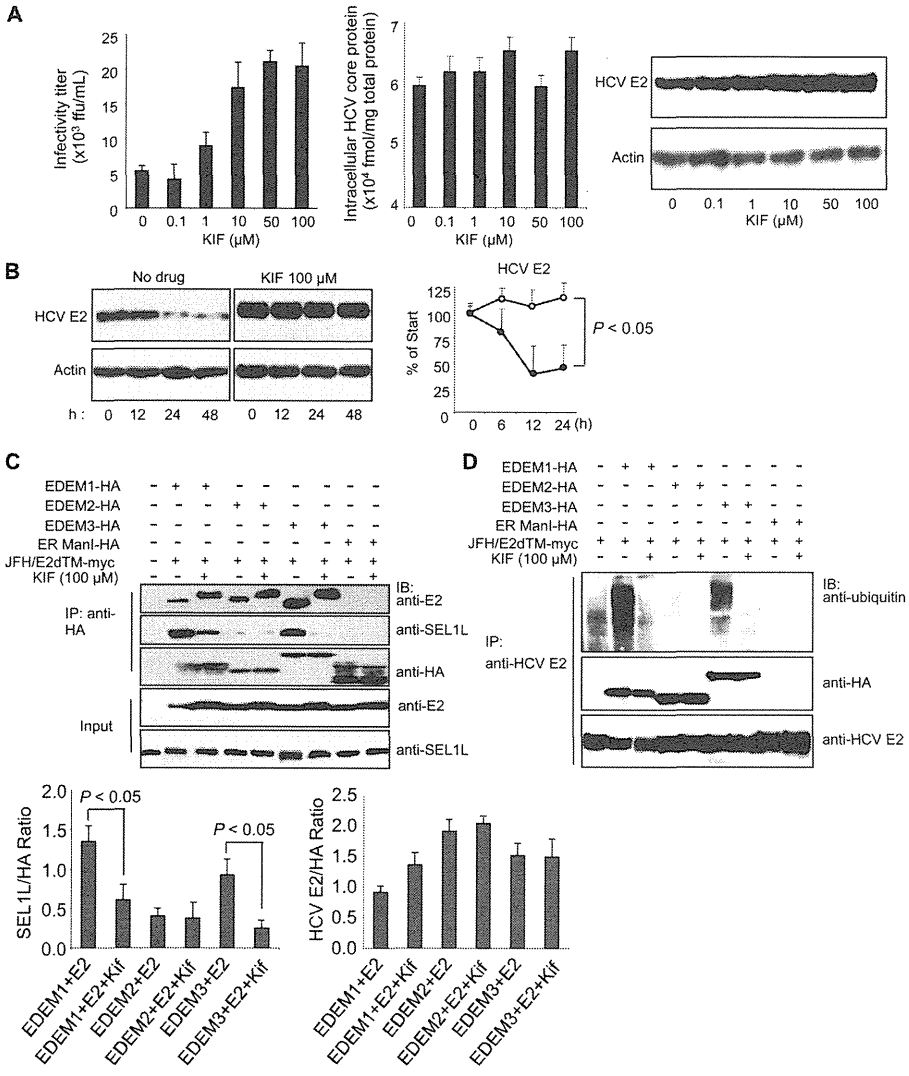

FIGURE 5. **Effect of KIF on HCV production and stability of E2.** *A*, extracellular HCV titer, intracellular HCV core protein expression, and steady-state level of HCV E2 in HuH-7 cells treated with different concentrations of KIF. *B*, CHX-based HCV protein stability assay of HCV E2 protein in KIF-treated cells as described in Fig. 3*E*. E2 protein levels normalized to actin levels are shown in the *graph* on the *right*. The *open* and *filled circles* indicate KIF-treated and nontreated cells, respectively. The mean ± S.D. (*error bars*) of two independent experiments are shown. *C*, binding of EDEMs and ER ManI with HCV E2 and SEL1L in 293T cells in the absence or presence of KIF. 293T cells were seeded in 6-well plates at a density of 3×10^5 cells/well. After overnight incubation, the cells were co-transfected with plasmids carrying HCV E2-myc (1 μg) and EDEM1-HA, EDEM2-HA, EDEM3-HA, or ER ManI-HA proteins (1 μg each). After 6 h, the culture medium was replaced with fresh or KIF-containing medium (100 μM). Forty-eight hours later, the cells were harvested and immunoprecipitated (*IP*) with anti-HA antibodies, after which Western blotting (*IB*) was performed with the indicated antibodies. Specific signals were quantified by densitometry, and the ratio between HCV E2 and HA (*right graph*) and between SEL1L and HA (*left graph*) in the same *lanes* is plotted on the graphs. The mean ± S.D. of three independent experiments are shown. *D*, EDEM protein-mediated ubiquitylation of HCV E2 protein in 293T cells in the absence or presence of KIF. The experimental procedure was the same as that described in Fig. 5*C*, except that immunoprecipitation was performed with anti-HCV E2 antibodies.

viruses is still unknown. To this end, we examined its role in the life cycle of JEV, another member of the Flaviviridae family. In contrast to HCV, KIF treatment had little effect on JEV production in infected cells (Fig. 6*A*) or the steady-state level of viral E glycoprotein (Fig. 6*B*). Interaction of EDEMs with JEV E was analyzed further. Neither EDEMs nor ER ManI was found to interact with JEV E in cells (Fig. 6*C*), indicating no significant role of the ERAD pathway in the JEV life cycle. Altogether, these results strongly suggest that the ERAD pathway is involved in the quality control of glycoproteins of specific viruses, possible through an interaction with EDEM(s), and subsequent regulation of virus production.

DISCUSSION

Accumulating evidence points to a role of the ERAD pathway in the pathogenesis of different genetic and degenerative diseases. However, the involvement of ERAD in the life cycle of viruses and infectious diseases remains poorly understood. Until recently, an experimental HCV cell culture infection system has been lacking such that studies evaluating the effect of HCV infection on the ERAD pathway were performed by either using HCV subgenomic replicons which lack structural proteins or by ectopic expression of one or multiple structural proteins (21, 22). However, this problem was solved by identifica-

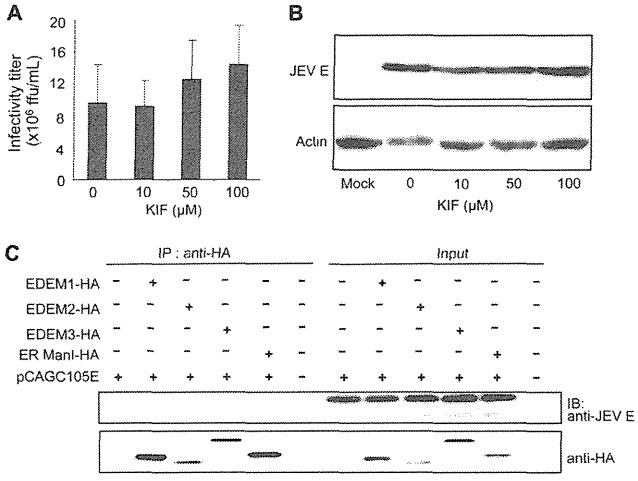

FIGURE 6. **Binding of JEV envelope glycoprotein with EDEMs and effect of KIF on JEV production.** *A*, JEV production in HuH-7 cells treated with KIF. The mean ± S.D. (*error bars*) of three independent experiments are shown. *B*, effect of KIF on the steady-state level of JEV envelope protein. *C*, binding of EDEMs with the JEV envelope.

tion of an HCV clone, JFH-1, capable of replicating and assembling infectious virus particles in cultured hepatocytes (15). In the present study, we used JFH-1 to examine the effect of HCV infection on activation of the ERAD pathway and its role in the virus life cycle. Our results show that the ERAD pathway is activated in HCV-infected cells, as evidenced by the maturation of XBP1 mRNA to its active form and up-regulation of EDEM1 (Fig. 1, *A–D*). Knocking down IRE1 reversed the induction of EDEM1, indicating that HCV infection-induced activation of the ERAD pathway is mediated through IRE1 (Fig. 1*F*). Loss- and gain-of-function analyses indicated that EDEM1 and EDEM3, particularly EDEM1, are involved in the post-translational control of HCV glycoproteins by which viral production is down-regulated (Figs. 3, *D* and *E*, and 4*A*). Our results suggest that EDEM1 and EDEM3 play a role in delivery of viral glycoproteins to the SEL1L-containing ubiquitin-ligase complex. It has recently been reported that coronavirus infection causes an accumulation of EDEM1 in membrane vesicles which are sites of viral replication, but that EDEM1 is not required for coronavirus replication (23). To our knowledge, the present study is the first to demonstrate regulation of the viral life cycle by ERAD machinery through interaction of EDEMs with viral glycoproteins.

We propose that the mechanisms described here are important during the early stages of establishing persistent HCV infection. ER stress caused by high levels of HCV infection during the acute phase presumably results in activation of the ERAD pathway. Induced EDEMs enhance the degradation of HCV envelope proteins, thereby reducing virus production. Maintenance of moderately low levels of HCV in the infected liver may contribute to the persistence of HCV infection, often associated with a lengthy asymptomatic phase that can last for decades. A range of viruses, including flaviviruses such as JEV, dengue virus, and West Nile virus, have been reported to induce XBP1 mRNA splicing triggered by ER stress (2, 3, 24). However, we demonstrate here that, in contrast to HCV, the envelope protein of JEV, which causes acute encephalitis, is not recognized by EDEMs, and the ERAD pathway does not control JEV production.

N-Linked glycoproteins displaying the glycan precursor Glc1Man9GlcNAc2 bind ER chaperones, such as calnexin or calreticulin, which facilitates protein folding. Removal of the terminal Glc from glycans disrupts this interaction with chaperones leading to Man trimming and delivery to ERAD machinery. A glucosyltransferase can transfer the terminal Man-linked Glc back to glycans, thereby allowing the "calnexin cycle" to continue until the glycoproteins are properly folded (for review, see Ref. 25). During this cycle, the decision of when to abandon additional folding attempts for immature polypeptides and to direct them instead toward the degradation pathway appears to be a crucial element of protein quality control. The basis by which this occurs, however, is not fully understood. Here, we demonstrate that stabilization of HCV envelope proteins and increased virus production occurs with KIF treatment (Fig. 5, *A* and *B*) and with gene silencing of either EDEM1 or EDEM3 (Figs. 3, *D* and *E*, and 4*A*). It is generally accepted that ERAD functions to eliminate proteins that are unable to adopt their native structure after translocation into the ER. From our results, however, one could argue that, during the HCV life cycle, at least a fraction of the competently folded viral glycoprotein intermediates may be released from the calnexin cycle before maturation and thereby be recognized as ERAD substrates. As suggested previously, the processes of protein folding and ERAD compete to some extent for newly synthesized polypeptides (26, 27). Under conditions in which high concentrations of ERAD-related factors are found in the ER due to induction of ER stress by viral infection, activated ERAD machinery may efficiently capture protein intermediates with folding/refolding capacity and cause premature termination of chaperone-assisted protein folding.

EDEM1 has recently been found to bind SEL1L, which is involved in the translocation of ERAD substrates from the ER to the cytoplasm (20). Our results demonstrate efficient binding of EDEM1 and EDEM3 to SEL1L, whereas EDEM2 exhibits only residual binding. In agreement with these results, increased ubiquitylation of HCV E2 protein was observed in cells overexpressing EDEM1 and EDEM3, but not in cells overexpressing the EDEM2 ortholog (Fig. 3*B*). Furthermore, KIF inhibited the binding of EDEM1 and EDEM3 with SEL1L, thus abrogating the ubiquitylation and enhancing the stability of HCV E2 protein (Fig. 5, *B* and *D*). It has been reported that KIF inhibits the interaction between EDEM1 and SEL1L, thus stabilizing ERAD substrates (4). Therefore, our results confirm previous findings and show that, along with EDEM1, KIF inhibits the binding of SEL1L to EDEM3. Furthermore, we have been the first to show that HCV E2 is a virus-derived ERAD substrate that can be used to analyze the mechanisms of this pathway. Taken together, our results indicate that EDEM1 and EDEM3, but not EDEM2, might be involved in targeting ERAD substrates to the translocation machinery, which may partly explain the different roles of the three EDEMs in HCV production. Although both EDEM1 and EDEM3 bind SEL1L and HCV envelope proteins, EDEM1 appears to have a larger role in regulation of HCV production than EDEM3. This is supported further by the finding that enhanced ubiquitylation of HCV E2 occurs in the presence

of EDEM1 overexpression (Figs. 3*B* and 5*D*). In EDEM3-knockdown cells, EDEM1 may take over the function of delivering ERAD substrates to the translocation machinery. We also speculate that EDEM1 may function as a helper for EDEM3. This is supported by the observation that EDEM1 and EDEM3 synergistically increase HCV production when knocked down together (data not shown). HCV glycoproteins are a suitable means by which to investigate differences and redundancies pertaining to the role of EDEMs in the ERAD pathway.

HCV-infected and TM-treated cells demonstrated the greatest activation of EDEM1 transcript production among EDEMs (Fig. 1, *C* and *D*, and supplemental Fig. S1). Although it is known that XBP1 binds to specific ER stress-responsive *cis*-acting elements to induce EDEMs (28, 29), the exact mechanism of transcriptional regulation is not fully understood. It will be interesting to examine regulatory mechanism(s) specific to individual EDEM homologs in an ER stress-dependent or -independent manner.

These findings highlight the crucial role of the ERAD pathway in the HCV life cycle. Further studies are needed to clarify the details of this complex pathway. The data generated in this work, however, further contribute to our understanding of the mechanisms that govern the maturation and fate of viral glycoproteins in the ER.

Acknowledgments—We thank Dr. F. V. Chisari for the HuH-7.5.1 cells, Drs. N. Hosokawa and K. Nagata for the EDEM expression plasmids, Dr. K. Mori for the reporter plasmids of GRP78 and GRP94, and Drs. C. K. Lim and T. Takasaki for the anti-JEV antibody. We thank Drs. Chia-Yi Yu and Yi-Ling Lin for valuable advice and T. Date, M. Kaga, M. Sasaki, and T. Mizoguchi for assistance.

REFERENCES

1. Vembar, S. S., and Brodsky, J. L. (2008) *Nat. Rev. Mol. Cell Biol.* **9,** 944–957
2. Yu, C. Y., Hsu, Y. W., Liao, C. L., and Lin, Y. L. (2006) *J. Virol.* **80,** 11868–11880
3. Barry, G., Fragkoudis, R., Ferguson, M. C., Lulla, A., Merits, A., Kohl, A., and Fazakerley, J. K. (2010) *J. Virol.* **84,** 7369–7377
4. Isler, J. A., Skalet, A. H., and Alwine, J. C. (2005) *J. Virol.* **79,** 6890–6899
5. Helenius, A., and Aebi, M. (2004) *Annu. Rev. Biochem.* **73,** 1019–1049
6. Mast, S. W., Diekman, K., Karaveg, K., Davis, A., Sifers, R. N., and Moremen, K. W. (2005) *Glycobiology* **15,** 421–436
7. Hirao, K., Natsuka, Y., Tamura, T., Wada, I., Morito, D., Natsuka, S., Romero, P., Sleno, B., Tremblay, L. O., Herscovics, A., Nagata, K., and Hosokawa, N. (2006) *J. Biol. Chem.* **281,** 9650–9658
8. Bartenschlager, R., and Lohmann, V. (2000) *J. Gen. Virol.* **81,** 1631–1648
9. Reed, K. E., and Rice, C. M. (2000) *Curr. Top. Microbiol. Immunol.* **242,** 55–84
10. Zhong, J., Gastaminza, P., Cheng, G., Kapadia, S., Kato, T., Burton, D. R., Wieland, S. F., Uprichard, S. L., Wakita, T., and Chisari, F. V. (2005) *Proc. Natl. Acad. Sci. U.S.A.* **102,** 9294–9299
11. Zhao, Z., Date, T., Li, Y., Kato, T., Miyamoto, M., Yasui, K., and Wakita, T. (2005) *J. Gen. Virol.* **86,** 2209–2220
12. Tani, H., Shiokawa, M., Kaname, Y., Kambara, H., Mori, Y., Abe, T., Moriishi, K., and Matsuura, Y. (2010) *J. Virol.* **84,** 2798–2807
13. Yoshida, H., Haze, K., Yanagi, H., Yura, T., and Mori, K. (1998) *J. Biol. Chem.* **273,** 33741–33749
14. Murakami, K., Kimura, T., Osaki, M., Ishii, K., Miyamura, T., Suzuki, T., Wakita, T., and Shoji, I. (2008) *J. Gen. Virol.* **89,** 1587–1592
15. Wakita, T., Pietschmann, T., Kato, T., Date, T., Miyamoto, M., Zhao, Z., Murthy, K., Habermann, A., Kräusslich, H. G., Mizokami, M., Bartenschlager, R., and Liang, T. J. (2005) *Nat. Med.* **11,** 791–796
16. Lim, C. K., Takasaki, T., Kotaki, A., and Kurane, I. (2008) *Virology* **374,** 60–70
17. Takeuchi, T., Katsume, A., Tanaka, T., Abe, A., Inoue, K., Tsukiyama-Kohara, K., Kawaguchi, R., Tanaka, S., and Kohara, M. (1999) *Gastroenterology* **116,** 636–642
18. Deng, L., Adachi, T., Kitayama, K., Bungyoku, Y., Kitazawa, S., Ishido, S., Shoji, I., and Hotta, H. (2008) *J. Virol. 82, 10375–10385*
19. Masaki, T., Suzuki, R., Saeed, M., Mori, K., Matsuda, M., Aizaki, H., Ishii, K., Maki, N., Miyamura, T., Matsuura, Y., Wakita, T., and Suzuki, T. (2010) *J. Virol. 84, 5824–5835*
20. Cormier, J. H., Tamura, T., Sunryd, J. C., and Hebert, D. N. (2009) *Mol. Cell* **34,** 627–633
21. Tardif, K. D., Mori, K., Kaufman, R. J., and Siddiqui, A. (2004) *J. Biol. Chem.* **279,** 17158–17164
22. Chan, S. W., and Egan, P. A. (2005) *FASEB J.* **19,** 1510–1512
23. Reggiori, F., Monastyrska, I., Verheije, M. H., Calì, T., Ulasli, M., Bianchi, S., Bernasconi, R., de Haan, C. A., and Molinari, M. (2010) *Cell Host Microbe* **7,** 500–508
24. Medigeshi, G. R., Lancaster, A. M., Hirsch, A. J., Briese, T., Lipkin, W. I., Defilippis, V., Früh, K., Mason, P. W., Nikolich-Zugich, J., and Nelson, J. A. (2007) *J. Virol.* **81,** 10849–10860
25. Molinari, M. (2007) *Nat. Chem. Biol.* **3,** 313–320
26. Eriksson, K. K., Vago, R., Calanca, V., Galli, C., Paganetti, P., and Molinari, M. (2004) *J. Biol. Chem.* **279,** 44600–44605
27. Wu, Y., Swulius, M. T., Moremen, K. W., and Sifers, R. N. (2003) *Proc. Natl. Acad. Sci. U.S.A.* **100,** 8229–8234
28. Olivari, S., Galli, C., Alanen, H., Ruddock, L., and Molinari, M. (2005) *J. Biol. Chem.* **280,** 2424–2428
29. Yoshida, H., Matsui, T., Hosokawa, N., Kaufman, R. J., Nagata, K., and Mori, K. (2003) *Dev. Cell* **4,** 265–271

Journal of Medical Virology 82:1545–1553 (2010)

Natural Killer Cells Target HCV Core Proteins During the Innate Immune Response in HCV Transgenic Mice

Kenichi Satoh,[1,2] Hiroki Takahashi,[2] Chiho Matsuda,[1] Toshiyuki Tanaka,[3] Masayuki Miyasaka,[4] Mikio Zeniya,[2] and Michinori Kohara[1]*

[1]*Department of Microbiology and Cell Biology, The Tokyo Metropolitan Institute of Medical Science, Bunkyo-ku, Tokyo, Japan*
[2]*Division of Gastroenterology and Hepatology, Department of Internal Medicine, The Jikei University School of Medicine, Minato-ku, Tokyo, Japan*
[3]*Laboratory of Immunobiology, Department of Pharmacy, School of Pharmacy, Hyogo University of Health Sciences, Chuo-ku, Kobe, Japan*
[4]*Laboratory of Immunodynamics, Department of Microbiology and Immunology, Osaka University Graduate School of Medicine, Suita, Osaka, Japan*

The mechanism of the innate immune response to hepatitis C virus (HCV) has not been fully elucidated, largely due to the lack of an appropriate model. We used HCV transgenic (Tg) mice, which express core, E1, E2, and NS2 proteins regulated by the Cre/*loxP* switching expression system, to examine the innate immune response to HCV structural proteins. Twelve hours after HCV transgene expression, HCV core protein levels in Tg mouse livers were 15–47 pg/mg. In contrast, in Tg mice with a depletion of natural killer (NK) cells, we observed much higher levels of HCV core proteins (1,597 pg/ml). Cre-mediated genomic DNA recombination efficiency in the HCV-Tg mice was strongly observed in NK cell-depleted mice between 0.5 and 1 day as compared to non-treated mice. These data indicated that NK cells participate in the elimination of core-expressing hepatocytes in the innate immune responses during the acute phase of HCV infection. ***J. Med. Virol. 82:1545–1553, 2010.***

KEY WORDS: HCV; Cre/loxP switching Tg; innate immunity; natural killer cell; core protein

INTRODUCTION

Although a variety of studies have demonstrated that infection with hepatitis C virus (HCV) elicits an innate immune response in human hosts, the mechanisms behind this response are not well understood. Details on the first step of the immune process might assist in the development of treatments for chronic hepatitis, cirrhosis, and hepatocellular carcinoma. One of the factors limiting such HCV immune research is the general lack of animal models: Humans are the only natural HCV host, and to date, chimpanzees are the only animals that have been infected with HCV.

Clinically, approximately 50% of symptomatic patients eliminate the virus, whereas in an asymptomatic course, more than 80% of acute HCV infections develop into chronic infection [Gerlach et al., 2003], indicating that the infected host's immune reaction may influence the course of the disease. In the chimpanzee model, HCV significantly induces type I interferon (IFN) [Bigger et al., 2001; Su et al., 2002]. However, this response occurs irrespective of the outcome of infection [Disson et al., 2004; Machida et al., 2001; Su et al., 2002; Thimme et al., 2002], and NS3-4A can inhibit RIG-1-mediated signaling, which is required to be activated for IFN production [Vilasco et al., 2006].

Natural killer (NK) cells constitute the first line of host defense against invading pathogens and are usually activated in the early phase of viral infection.

Abbreviations used: HCV, hepatitis C virus; NK cell, natural killer cell; IFN, interferon; Tg, transgenic; ALT, alanine aminotransferase; IRF, interferon regulatory factor.

Grant sponsor: Ministry of Education, Culture, Sports, Science and Technology of Japan; Grant sponsor: Program for Promotion of Fundamental Studies in Health Sciences of the National Institute of Biomedical Innovation of Japan; Grant sponsor: Ministry of Health, Labor and Welfare of Japan.

*Correspondence to: Michinori Kohara, PhD, Department of Microbiology and Cell Biology, The Tokyo Metropolitan Institute of Medical Science, 2-1-6 Kamikitazawa, Setagaya-ku, Tokyo 156-8506, Japan. E-mail: kohara-mc@igakuken.or.jp

Accepted 28 April 2010
DOI 10.1002/jmv.21859
Published online in Wiley InterScience (www.interscience.wiley.com)

The liver is particularly enriched with NK cells, which are activated by hepatotropic viruses such as HCV. There have been some reports of the association between NK cells and HCV [Ebihara et al., 2008; Knapp et al., 2009; Vidal-Castineira et al., 2010]. For instance, NK cell numbers were consistently lower in individuals with persistent HCV infections [Golden-Mason et al., 2008]. Additionally, the function of NK cells can be inhibited by HCV proteins such as envelope protein E2, which impairs the effector function of NK cells by interacting with CD81 on their surface [Crotta et al., 2002; Tseng and Klimpel, 2002].

Most of these studies on the association between NK cells and HCV have been performed during the chronic phase of HCV infection. To our knowledge, there has been no research on the innate immune response during the acute phase of HCV infection, because of the difficulty in analyzing early immune reactions and the lack of appropriate animal models. Here, we have overcome this difficulty by using the Cre/*loxP* system to create a mouse model with conditional HCV transgene expression. This allowed us to analyze HCV-specific innate immunity.

MATERIALS AND METHODS

HCV Transgenic Mice

HCV-Tg mice CN2-8 and CN2-29 (BALB/c, 9- to 12-week old) were used in the experiments. These two Tg mice lineages possess HCV genotype 1b, which is regulated by the Cre/*loxP* conditional switching system [Wakita et al., 1998]. NK cell- and $CD8^+$ T-cell-deficient HCV-Tg mice were also established by mating HCV-Tg mice with syngenic IRF-1-deficient mice, in which a strong reduction in NK cells [Duncan et al., 1996; Ohteki et al., 1998] and $CD8^+$ T cells [Matsuyama et al., 1993] has been reported.

All mice were cared for according to the guidelines of the NIH Guide for the Care and Use of Laboratory Animals.

Structure of CALCN2, the Cre-Mediated Activation Transgene Unit

R6CN2 HCV cDNA (nucleotides: 294–3,435, aa: 1–1,013) contains the core, E1, E2, and NS2 regions. This construct does not lead to HCV mRNA transcription before recombination. It was cloned downstream of the CAG promoter, neomycin-resistant gene (*neo*), and poly(A) signal; the latter two of these were flanked by *loxP* sequences. The CAG promoter comprises, in order, the cytomegalovirus enhancer, actin promoter, and the globin poly(A) signal. CALNCN2, the Cre-mediated activation transgene unit, consists of the CAG promoter, a *loxP* sequence, the *neo*-resistance gene, the SV40 poly(A) signal, a second *loxP* sequence, R6CN2 HCV cDNA, and the globin poly(A) signal, in that order.

Upon recognition of the *loxP* site, Cre recombinase deletes the neo gene and the SV40 poly(A) signal, along with one of the *loxP* sequences. It then ligates the CAG promoter to the HCV cDNA and the globin poly(A) signal. This genomic structure alteration enables the production of HCV mRNA [Wakita et al., 1998].

Hydrodynamics-Based Transfection of Naked Plasmid DNA

Cre recombinase cDNA (pCAN-Cre/pBR325 plasmid) was cloned downstream of the CMV promoter. Plasmid DNA was prepared using the triton-cesium chloride method. Plasmid DNA (20 μg) was diluted with 2.0 ml of PBS(−) mixed with atelocollagen (KOKENCELLGEN I-AC; Koken, Tokyo, Japan) [Ochiya et al., 2001; Minakuchi et al., 2004] to a final concentration of 0.01%. This was then injected via a tail vein, after which it entered circulation within 6–8 sec [Liu et al., 1999].

Depletion of NK Cells

Transgenic mice were treated intraperitoneally with 1 mg of anti-IL2 receptor-β monoclonal antibody (TM-βI, rat IgG2b) [Tanaka et al., 1993] in 500 μl of PBS(−) once, 2 days before Cre/loxP switching.

Quantification of HCV Core Proteins in Mouse Livers

Hepatocyte HCV core protein concentrations were quantified with a fluorescent enzyme immunoassay (FEIA) by using HCV core monoclonal antibodies from a commercial kit, as previously described [Kashiwakuma et al., 1996].

Immunoblot Analysis

Liver tissues (100–150 μg) were lysed with 300 μl of RIPA buffer (1% SDS, 0.5% Nonidet P40, 0.5 mmol/L EDTA, 150 mmol/L NaCl, and 1 mmol/L DTT and 10 mmol/L Tris, pH 7.4). After the supernatant protein concentration was determined, 30 μg of total protein was electrophoresed on SDS–PAGE (15% polyacrylamide) and transferred to a polyvinylidene difluoride (PVDF) membrane (Immobilon-P, Millipore, Bedford, MA). The membrane was incubated with biotinylated 515S (an anti-HCV core monoclonal antibody), 384 (an anti-HCV E1 monoclonal antibody), or 541 (an anti-HCV E2 monoclonal antibody) [Tsukiyama-Kohara et al., 2004], followed by horseradish peroxidase-conjugated streptavidin. Proteins were visualized using the ECL system (Amersham Biosciences, Cleveland, OH).

Southern Blotting

Genomic DNA (4 μg) was extracted from mouse liver tissue by using the phenol–chloroform method. It was digested with *Xba*I and then resolved by electrophoresis on a 0.8% agarose gel. Bands were transferred to a Hybond-N membrane (Amersham Biosciences) by using the Vacugene 2016 (LKB Biotechnology, Bromma, Sweden). The blots were then probed with a ^{32}P-dCTP-

labeled CALNCN2 (nucleotides: 483–1,389) probe. The probe was generated using a Random Primer DNA Labeling Kit, Ver 2.0 (Takara, Shiga, Japan).

Northern Blotting

Total RNA (30 μg) was extracted from mouse liver tissue by using the AGPC method. Bands were transferred to a Hybond-N membrane (Amersham Biosciences). The blots were then probed with the same probe used for Southern blotting.

Expression Plasmids of HCV Structural Proteins

We generated expression plasmids of HCV-core (aa: 1–192; pEF-core), HCV-E1 (aa: 168–383; pEF-E1), and HCV-E2 (aa: 367–830; pEF-E2) [Takaku et al., 2003] under the control of the EF2-α promoter, and HCV-CN2 (aa: 1–1,013; pCAL CN2) [Tsukiyama-Kohara et al., 2004] and β-lactamase (pCAL-LacZ), under the control of the CAG promoter.

Cytokine Assay

Secretion of serum IFN-γ [Carroll et al., 1997], IL-12, and TNF-α was measured using enzyme-linked immunosorbent assay kits (BioSource, Camarillo, CA), according to the manufacturer's protocols.

Assay of Alanine Aminotransferase (ALT) Levels

Serum ALT concentrations were determined with a Transferase Nissui kit (Nissui Pharmaceutical Co., Tokyo, Japan) and then standardized and expressed as IU/L.

RESULTS

HCV Core Protein and ALT Levels During the Early Phase of HCV Transgenic Mouse

In CN2-8 Tg mice, HCV core protein expression levels were as follows: day 0.5: 15 ± 16 pg/mg; day 1: 175 ± 96 pg/mg; day 2: 207 ± 77 pg/mg; day 3: 33 ± 41 pg/mg; day 4: 431 ± 256 pg/mg; day 14: 4 ± 1 pg/mg (Fig. 1A). In the CN2-29 Tg mice, HCV core protein expression levels were as follows: day 0.5: 47 ± 13 pg/mg; day 1: 495 ± 165 pg/mg; day 2: 1189 ± 210 pg/mg; day 3: 26 ± 39 pg/mg; day 4: 59 ± 49 pg/mg; day 14: 2 ± 2 pg/mg (Fig. 1B). ALT levels were 489 ± 150 IU/L in the CN2-8 Tg mice and 2,282 ± 358 IU/L in the CN2-29 Tg mice at day 0.5, after which the levels quickly decreased. In both mice lineages, HCV core protein expression levels were low from day 8. In contrast, HCV core protein was not detected and the ALT levels were low (357 ± 150 IU/L) at day 0.5 in the CN2-29 Tg mice injected with the negative control vector (pBR325) (Fig. 1C).

In the immunoblot analysis, the HCV core (21 kDa) protein was detectable from days 0.5 to 3 (Fig. 1D). To investigate why the core protein was eliminated after day 3, we performed Southern and Northern blot analyses using liver tissue extracts. Transgene recombination occurred in the Tg mouse livers (Fig. 1E). CALNCN2 mRNA expression levels were similar throughout the study period (Fig. 1F). Although HCV mRNA was consistently observed, the HCV core protein was eliminated by day 4 (Fig. 1D), suggesting that some immune factors were active against HCV core protein from day 3 onward.

Histopathology of the HCV Protein Expressed During the Early Phase of HCV Transgenic Mouse

Histopathology of the CN2-29 Tg mice (Fig. 2B–E) revealed inflammation and elevation of ALT levels in livers with HCV structural protein expression compared to that in livers without HCV structural protein expression (Fig. 2F–I). The presence of HCV structural proteins was associated with the following: hepatocyte necrosis and mononuclear cell infiltration in both the liver lobules and in the periportal area, on day 0.5 (Fig. 2B); mononuclear cell infiltration, on days 1 (Fig. 2C) and 3 (Fig. 2E); and Kupffer-like infiltrated cells, on day 2 Fig. 2D). No changes in inflammation were found in the control vector-injected mice (Fig. 2F–I).

NK Cell Activity Against Cells Expressing HCV Proteins

HCV core protein expression levels were higher in the CN2-8 IRF-1 knockout mice than in wild-type Tg mice (309 ± 76 pg/mg vs. 15 ± 16 pg/mg), while ALT levels were lower (194 ± 53 I/U vs. 489 ± 142 IU/L; Fig. 1A).

HCV core protein expression levels were higher in NK cell-depleted mice with anti-IL2 receptor-β antibodies than in non-treated CN2-29 Tg mice (1,597 ± 153 pg/mg vs. 47 ± 13 pg/mg), while ALT levels were lower (608 ± 258 IU/L vs. 2,282 ± 458 IU/L) on day 0.5 (Figs. 1B and 3). However, core protein levels were drastically reduced in the treated mice on day 2. Transgene recombination was strongly observed between days 0.5 and 1 (Fig. 3C), indicating that activated NK cells were responsible for eradicating the HCV proteins.

In BALB/c mice whose livers had been hydrodynamically transfected with the pCAL-CN2 plasmid, HCV core protein expression level was 123 ± 45 pg/mg and the ALT level was 3,256 ± 703 IU/L on day 0.5. By day 1, both the HCV core protein expression level (54 ± 65 pg/mg) and the ALT level (841 ± 174 IU/L) had decreased; they were also relatively low on day 2 (Fig. 4A).

Both the HCV core protein expression level (2,900 ± 400 pg/mg on days 0.5 and 10,700 ± 3,100 pg/mg on day 1) and the ALT level (295 ± 197 IU/L on day 0.5 and 91 ± 51 IU/L on day 1) were lower in IRF-1 knockout BALB/c mice than in wild-type BALB/c mice (Fig. 4A,B). In contrast, in wild-type BALB/c mice hydrodynamically transfected with the pCAL-LacZ plasmid, the β-galactosidase level did not dramatically change over the study period (7.9 ± 2.0 on day 0.5; 3.9 ± 2.1 on day 14). The ALT level (450 ± 90 IU/L) was lower in plasmid-transfected mice than in wild-type mice (Fig. 4A,C), but

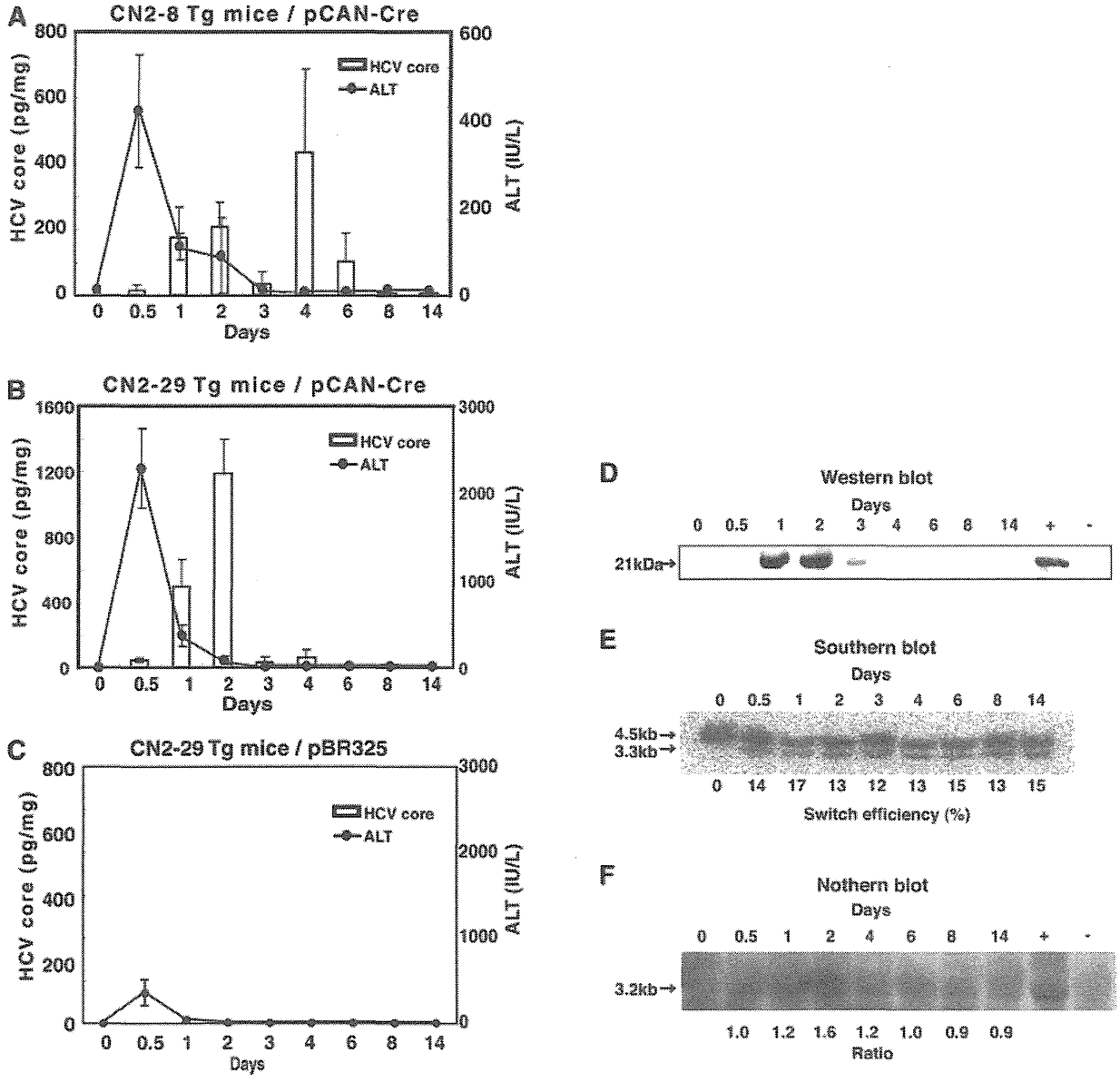

Fig. 1. Quantification of HCV core protein production and ALT levels in transgenic mice hydrodynamically transfected with the pCAN-Cre plasmid. Values for core protein and serum ALT levels represents the mean and SD from three experiments. **A**: CN2-8 transgenic mice. Analysis of quantity of core protein and serum ALT levels in the hepatocytes. Hepatitis was first detectable via elevated serum ALT activity on day 0.5, after which ALT activity rapidly rose, only to return to the baseline level after day 3. Hepatocyte core protein levels peaked twice, on day 2 (207 ± 77 pg/mg) and day 4 (431 ± 256 pg/mg). **B**: CN2-29 transgenic mice. Hepatitis was first detectable as elevated serum ALT activity on day 0.5. Serum ALT activity peaked at 2,282 ± 358 IU/L and then declined gradually from day 1 (366 ± 123 IU/L). It returned to the baseline level after day 2. Hepatocyte core protein levels were first detectable on day 0.5 (47 ± 13 pg/mg), peaked on day 2 (1,189 ± 210 pg/mg), and returned to the baseline level after day 3. **C**: Serum ALT levels in negative control plasmids (pBR325, 20 μg) injected into CN2-29 transgenic mice. The serum ALT level of the control plasmids was lower than in CN2-29 transgenic mice and was only detectable on day 0.5, after which it returned to the baseline level. Core protein levels were not detectable. **D**: Immuno-blot from the liver of a CN2-29 transgenic mouse liver hydrodynamically transfected with the pCAN-Cre plasmid. HCV core protein in the liver extract was barely detectable 12 h after switching in the CN2-29 Tg mouse, was strongly detected on days 1 and 2, and was eliminated after day 3. The density of the HCV core protein band reflected the HCV protein expression levels shown in Fig. 1B. **E**: Switching efficiency of Cre-mediated genomic DNA recombination in the liver of a CN2-29 transgenic mouse hydrodynamically transfected with the pCAN-Cre plasmid. HCV transgene recombination in the somatic tissues of pCANCre-injected mice. Southern blot analysis of tissues from CN2-29 mice. Transgene recombination was consistently observed between days 0.5 and 14. kb, kilobase pairs. **F**: Cre-mediated genomic DNA recombination and mRNA in the CN2-29 transgenic mouse liver hydrodynamically transfected with the pCAN-Cre plasmid. The expression level of CALNCN2 mRNA by Northern blot analysis.

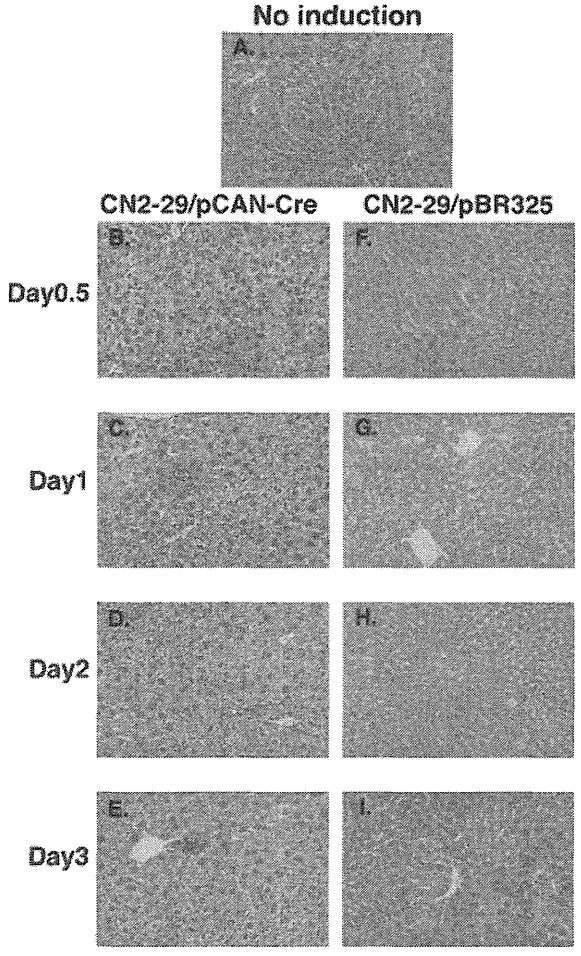

Fig. 2. Hematoxylin and eosin staining of liver sections from CN2-29 Tg mice. The presence of HCV structural proteins was associated with the following: (**B**) hepatocyte necrosis and mononuclear cell infiltration in the liver lobules and periportal area on day 0.5; (**C,E**) mononuclear cell infiltration on days 1 and 3; (**D**) Kupffer-like cell infiltration on day 2. **F–I**: No inflammation changes were seen in the liver following pBR325 plasmid injection.

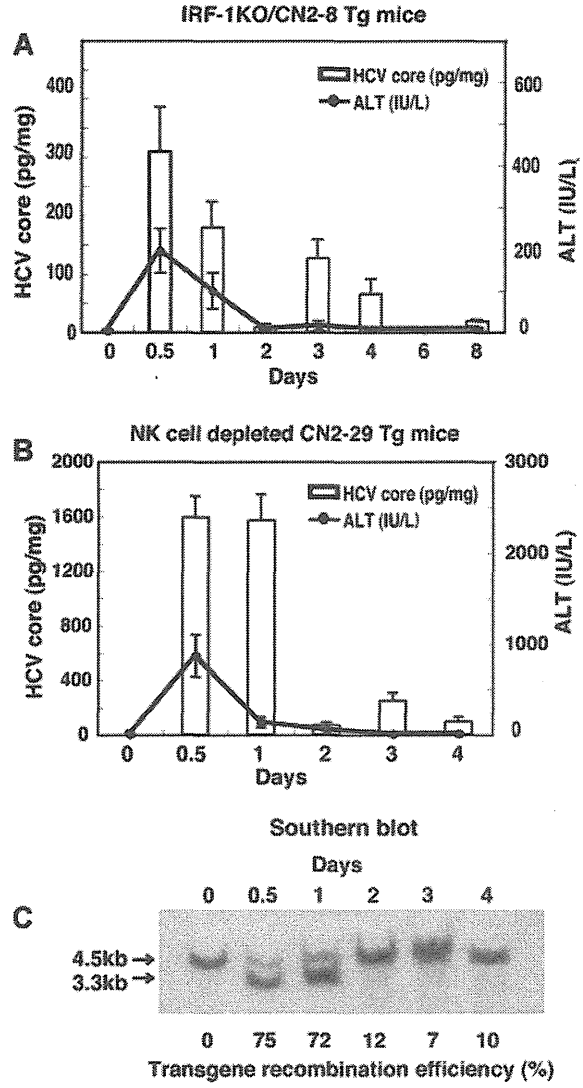

Fig. 3. Quantification of HCV core protein production and serum ALT levels in IRF-1 knockout CN2-8 transgenic mice and NK cell-depleted CN2-29 transgenic mice hydrodynamically transfected with the pCAN-Cre plasmid. **A**: HCV core protein and serum ALT levels in IRF-1 knockout CN2-8 Tg mice. The core protein level in the hepatocytes rapidly increased on day 0.5 (309 ± 76 pg/mg). The serum ALT level (194 ± 53 IU/L) was lower than in wild-type mice (490 ± 150 IU/L) on day 0.5 (Fig. 1A). **B**: HCV core protein and serum ALT levels in NK cell-depleted CN2-29 Tg mice. The core protein level in the liver rapidly increased on day 0.5 ($1,597 \pm 153$ pg/mg). The serum ALT level (489 ± 142 IU/L) was lower than in wild-type mice ($2,282 \pm 358$ IU/L) on day 0.5 (Fig. 1B). **C**: Cre-mediated genomic DNA recombination efficiency throughout the study period.

the β-galactosidase level (7.4 ± 2.5 on day 0.5 and 5.4 ± 2.3 on day 1) was comparable. Finally, the ALT level was 325 ± 178 IU/L on day 0.5 (Fig. 4D).

When the pCAN-Cre/pBR325 plasmid was injected into wild-type BALB/c mice, the results were similar to those seen in the absence of the vector (data not shown), suggesting that the pCAN-Cre plasmid injection had no effect.

Cumulatively, these findings suggest that HCV protein-expressing cells were eliminated by NK cells during the acute early phase of innate immunity.

IFN-γ Secretion Induced HCV Core Protein in the Acute Early Phase of Innate Immunity

We analyzed cytokine (IFN-γ, IL-12, and TNF-α levels from days 0 to 14 after the hydrodynamic transfection of pCAN-Cre plasmids into CN2-29 Tg mice. Serum IL-12 and TNF-α were not detected on any day during the study period (data not shown). Serum IFN-γ was detected on day 0.5 in pCAN-Cre-transfected mice, but not in control vector-injected mice (Fig. 5A).

IFN-γ was strongly secreted on day 0.5 in response to transfection with pEF-core expression plasmids (Fig. 5B), but was only slightly induced by the HCV E1 and E2 (not detected) proteins (Fig. 5B). In contrast,

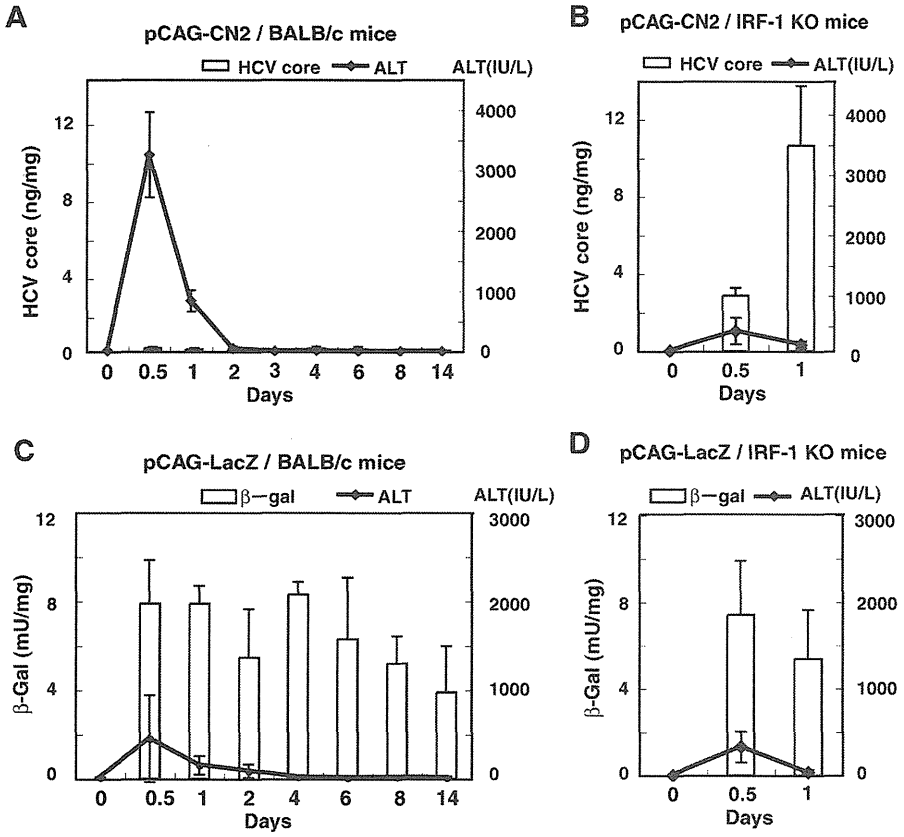

Fig. 4. Quantification of HCV core protein production and serum ALT levels in wild-type BALB/c mice and IRF-1 knockout BALB/c mice hydrodynamically transfected with expression plasmids. **A**: Results for wild-type BALB/c mice injected with pCAG-CN2 (Fse). HCV core protein in the liver was barely detectable at day 0.5 (0.123 ± 0.045 ng/mg) and declined gradually thereafter. The serum ALT level peaked on day 0.5 ($3{,}256 \pm 703$ IU/L) and declined gradually thereafter. **B**: Results for IRF-1 knock out BALB/c mice injected with pCAG-CN2 (Fse). HCV core protein levels in the hepatocytes was most strongly detected on days 0.5 (2.9 ± 0.4 ng/mg) and 1 (10.7 ± 3.1 ng/mg). Serum ALT was suppressed on day 0.5 (295 ± 197 IU/L). **C**: Results for BALB/c mice injected with pCAG-LacZ. Liver β-gal levels were first detectable on day 0.5 (7.9 ± 2.0 mU/mg) and were consistently detectable until day 14 (3.9 ± 2.1 mU/mg). The serum ALT level (450 ± 490 IU/L) was lower than that shown in Figure 2A ($3{,}256 \pm 703$ IU/L) at day 0.5, and returned to the baseline level after day 2. **D**: Results from IRF-1 knockout BALB/c mice injected with pCAG-LacZ. Liver β-gal levels were detected on days 0.5 (7.4 ± 2.5 mU) and 1 (5.4 ± 2.3 mU). The serum ALT level was (352 ± 178 IU/L) on day 0.5.

serum IFN-γ was not detected after transfection with pEF-core expression plasmids in CN2-8 IRF-1 (Fig. 5C). Serum IFN-γ secretion was suppressed in NK cell-depleted CN2-29 Tg mice and was not stimulated by pCAL-LacZ plasmid injection (Fig. 5D,E).

DISCUSSION

Immune responses to HCV during the acute phase of infection might play a crucial role in determining whether HCV is eliminated or is able to persist in the body. However, acute HCV infection is rarely symptomatic, making it tremendously difficult to analyze in vivo. In the present study, we generated an acute HCV model for the first time by using Tg mice with conditional expression regulated by the Cre/*loxP* system. Because there were no viral vector effects, we were able to observe HCV-specific innate immunity by using hydrodynamic transfection techniques.

NK cells constitute the first line of host defense against invading pathogens. Activated NK cells play an essential role in recruiting virus-specific T cells and inducing antiviral immunity in the liver [French et al., 2003]. They also eliminate virus-infected hepatocytes directly by cytolytic mechanisms and indirectly by secreting cytokines, which induce an antiviral state in host cells. In vitro studies revealed that NK cells are activated by cytokines during acute HCV infection [Yoon et al., 2008] and play an important antiviral role by eliminating the virus, both by killing it directly and by producing cytokines such as IFN-γ [Golden-Mason and Rosen, 2006].

In the present study, hepatocyte necrosis and intrahepatic mononuclear cell infiltration were observed on days 0.5 and 1 in wild-type mice. These were associated with elevated levels of serum ALT and IFN-γ and with reduced levels of HCV core protein expression. In contrast, NK cell depletion by IRF-1 knockout or treatment with anti-IL-2 receptor-β antibody was

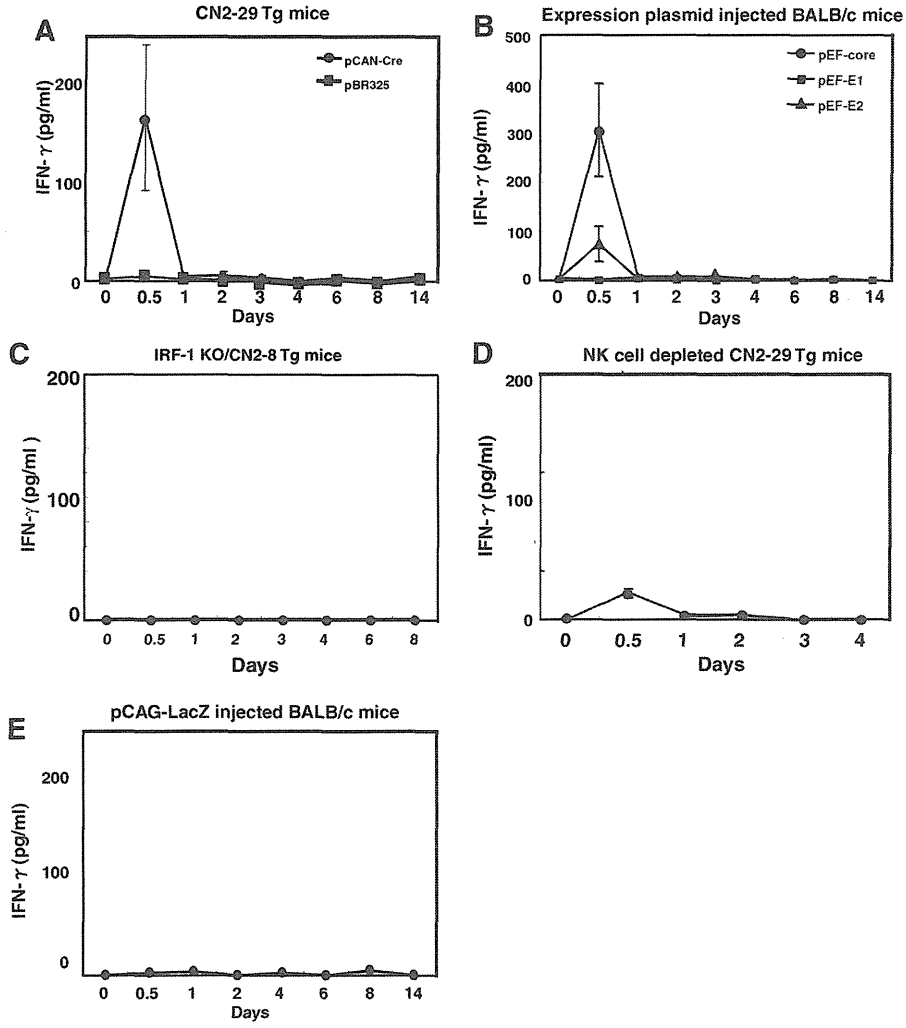

Fig. 5. Serum IFN-γ levels. **A**: Serum IFN-γ levels in CN2-29 Tg mice injected with the pCAN-Cre plasmid. Serum IFN-γ (168 ± 62 pg/ml) was detectable on day 0.5 in the pCAN-Cre plasmid-injected CN2-29 Tg mice (circle), but was not detectable in the pBR325 plasmid-injected CN2-29 Tg mice (square). **B**: Serum IFN-γ levels in mice injected with pEF-core (circle), -E1 (square), and -E2 (triangle) plasmids. **C**: Serum IFN-γ levels in IRF-1 knockout CN2-8 Tg mice injected with the pCAN-Cre plasmid. **D**: Serum IFN-γ levels in NK cell-depleted CN2-29 Tg mice injected with the pCAN-Cre plasmid. **E**: Serum IFN-γ levels in BALB/c mice injected with the pCAL-LacZ plasmid.

accompanied by increases in HCV core protein expression and decreased levels of ALT and IFN-γ on days 0.5 and 1. These results were confirmed by our histological observations. Cumulatively, these data suggest that the activity of NK cells might be directly cytolytic; specifically, they appear to play a significant role in IFN-γ secretion and elimination of virus-infected hepatocytes—especially core protein-presented hepatocytes—during the early phase of infection (days 0–1). Since the number of CD8+ cytotoxic T cells is greatly reduced in CN2-8 IRF-1 knockout mice, T cells usually participate in innate immunity, rather than acquired immunity. It has previously been reported that NK cells are required to recruit virus-specific T cells in response to HCV infection [Ahmad and Alvarez, 2004; Irshad et al., 2008]. These reports, together with our current work, indicate that NK cells play a very important antiviral role during acute HCV infection.

According to the results of the Southern and Northern blot analyses, non-cytolytic HCV core protein elimination takes place from days 3 to 14. However, this does not appear to be associated with IFN-γ or CD8+ cytotoxic T cells. Thus, during this period, another immune factor might be involved in eliminating HCV core protein in the hepatocytes without elevating ALT activity.

It is interesting that HCV core protein, but not E1 or E2 protein, induced the elevation of IFN-γ. Since HCV core protein is reported to activate NF-kB, thereby inducing the cellular inflammatory response [Dolganiuc et al., 2004], there is a possibility that HCV core protein

itself participates in the elevation of IFN-γ. IFN-γ is known to be expressed in the liver when infections spontaneously clear [Major et al., 2002; Thimme et al., 2002] and to be involved in the non-cytolytic control of HCV-infected hepatocytes [Thimme et al., 2001]. Additionally, IFN-γ inhibits the replication of subgenomic HCV replicons [Lohmann et al., 1999; Blight et al., 2000] in tissue culture cells [Frese et al., 2002; Lanford et al., 2003]. Since NK cells produce a large amount of IFN-γ when they are activated in response to inflammation, such as that caused by acute viral infection, both NK cells and IFN-γ may contribute to the innate immune response during acute HCV infection.

In conclusion, this Tg mouse model permits analysis of the HCV-specific immune response while avoiding adenovirus which has been applied for the study of HCV immunity. By using this model, we could determine some of the potential roles of NK cells in response to the presence of HCV structural protein during the early naïve phase of HCV infection. These findings confirm that NK cell activity is crucial in eliminating HCV-infected hepatocytes. This suggests that a potential new therapeutic approach is activation of NK cells in order to restore the innate immune defenses that control HCV replication.

ACKNOWLEDGMENTS

The authors wish to express their gratitude to Izumu Saito for his kind gift of the pCAN-Cre plasmid. We thank Dr. Masahiro Shuda for helpful comments during the preparation of this manuscript. We also thank Mitsugu Takahashi for breeding the transgenic mice.

REFERENCES

Ahmad A, Alvarez F. 2004. Role of NK and NKT cells in the immunopathogenesis of HCV-induced hepatitis. J Leukoc Biol 76:743–759.

Bigger CB, Brasky KM, Lanford RE. 2001. DNA microarray analysis of chimpanzee liver during acute resolving hepatitis C virus infection. J Virol 75:7059–7066.

Blight KJ, Kolykhalov AA, Rice CM. 2000. Efficient initiation of HCV RNA replication in cell culture. Science 290:1972–1974.

Carroll JM, Crompton T, Seery JP, Watt FM. 1997. Transgenic mice expressing IFN-gamma in the epidermis have eczema, hair hypopigmentation, and hair loss. J Invest Dermatol 108:412–422.

Crotta S, Stilla A, Wack A, D'Andrea A, Nuti S, D'Oro U, Mosca M, Filliponi F, Brunetto RM, Bonino F, Abrignani S, Valiante NM. 2002. Inhibition of natural killer cells through engagement of CD81 by the major hepatitis C virus envelope protein. J Exp Med 195:35–41.

Disson O, Haouzi D, Desagher S, Loesch K, Hahne M, Kremer EJ, Jacquet C, Lemon SM, Hibner U, Lerat H. Impaired clearance of virus-infected hepatocytes in transgenic mice expressing the hepatitis C virus polyprotein. Gastroenterology 2004. 126:859–872.

Dolganiuc A, Oak S, Kodys K, Golenbock DT, Finberg RW, Kurt-Jones E, Szabo G. 2004. Hepatitis C core and nonstructural 3 proteins trigger toll-like receptor 2-mediated pathways and inflammatory activation. Gastroenterology 127:1513–1524.

Duncan GS, Mittrucker HW, Kagi D, Matsuyama T, Mak TW. 1996. The transcription factor interferon regulatory factor-1 is essential for natural killer cell function *in vivo*. J Exp Med 184:2043–2048.

Ebihara T, Shingai M, Matsumoto M, Wakita T, Seya T. 2008. Hepatitis C virus-infected hepatocytes extrinsically modulate dendritic cell maturation to activate T cells and natural killer cells. Hepatology 48:48–58.

French AR, Yokoyama WM. 2003. Natural killer cells and viral infections. Curr Opin Immunol 15:45–51.

Frese M, Schwarzle V, Barth K, Krieger N, Lohmann V, Mihm S, Haller O, Bartenschlager R. 2002. Interferon-gamma inhibits replication of subgenomic and genomic hepatitis C virus RNAs. Hepatology 35:694–703.

Gerlach JT, Diepolder HM, Zachoval R, Gruener NH, Jung MC, Ulsenheimer A, Schraut WW, Schirren CA, Waechtler M, Backmund M, Pape GR. 2003. Acute hepatitis C: High rate of both spontaneous and treatment-induced viral clearance. Gastroenterology 125:80–88.

Golden-Mason L, Madrigal-Estebas L, McGrath E, Conroy MJ, Ryan EJ, Hegarty JE, O'Farrelly C, Doherty DG. 2008. Altered natural killer cell subset distributions in resolved and persistent hepatitis C virus infection following single source exposure. Gut 57:1121–1128.

Golden-Mason L, Rosen HR. 2006. Natural killer cells: Primary target for hepatitis C virus immune evasion strategies? Liver Transpl 12:363–372.

Irshad M, Khushboo I, Singh S, Singh S. 2008. Hepatitis C virus (HCV): A review of immunological aspects. Int Rev Immunol 27:497–517.

Kashiwakuma T, Hasegawa A, Kajita T, Takata A, Mori H, Ohta Y, Tanaka E, Kiyosawa K, Tanaka T, Tanaka S, Hattori N, Kohara M. 1996. Detection of hepatitis C virus specific core protein in serum of patients by a sensitive fluorescence enzyme immunoassay (FEIA). J Immunol Methods 190:79–89.

Knapp S, Warshow U, Hegazy D, Brackbury L, Guha IN, Fowell A, Little AM, Alexander GJ, Rosenberg WM, Cramp ME, Khakoo SI. 2009. Consistent beneficial effects of killer cell immunoglobulin-like receptor 2DL3 and group 1 human leukocyte antigen-C following exposure to hepatitis C virus. Hepatology 51:1–8.

Lanford RE, Guerra B, Lee H, Averett DR, Pfeiffer B, Chavez D, Notvall L, Bigger C. 2003. Antiviral effect and virus-host interactions in response to alpha interferon, gamma interferon, poly(i)-poly(c), tumor necrosis factor alpha, and ribavirin in hepatitis C virus subgenomic replicons. J Virol 77:1092–1104.

Liu F, Song Y, Liu D. 1999. Hydrodynamics-based transfection in animals by systemic administration of plasmid DNA. Gene Ther 6:1258–1266.

Lohmann V, Korner F, Koch J, Herian U, Theilmann L, Bartenschlager R. 1999. Replication of subgenomic hepatitis C virus RNAs in a hepatoma cell line. Science 285:110–113.

Machida K, Tsukiyama-Kohara K, Seike E, Tone S, Shibasaki F, Shimizu M, Takahashi H, Funata N, Taya C, Yonekawa H, Kohara M. 2001. Inhibition of cytochrome c release in Fas-mediated signaling pathway in transgenic mice induced to express hepatitis C viral proteins. J Biol Chem 276:12140–12146.

Major ME, Mihalik K, Puig M, Rehermann B, Nascimbeni M, Rice CM, Feinstone SM. 2002. Previously infected and recovered chimpanzees exhibit rapid responses that control hepatitis C virus replication upon rechallenge. J Virol 76:6586–6595.

Matsuyama T, Kimura T, Kitagawa M, Pfeffer K, Kawakami T, Watanabe N, Kundig TM, Amakawa R, Kishihara K, Wakeham A. 1993. Targeted disruption of IRF-1 or IRF-2 results in abnormal type I IFN gene induction and aberrant lymphocyte development. Cell 75:83–97.

Minakuchi Y, Takeshita F, Kosaka N, Sasaki H, Yamamoto Y, Kouno M, Honma K, Nagahara S, Hanai K, Sano A, Kato T, Terada M, Ochiya T. 2004. Atelocollagen-mediated synthetic small interfering RNA delivery for effective gene silencing *in vitro* and *in vivo*. Nucleic Acids Res 32:e109.

Ochiya T, Nagahara S, Sano A, Itoh H, Terada M. 2001. Biomaterials for gene delivery: Atelocollagen-mediated controlled release of molecular medicines. Curr Gene Ther 1:31–52.

Ohteki T, Yoshida H, Matsuyama T, Duncan GS, Mak TW, Ohashi PS. 1998. The transcription factor interferon regulatory factor 1 (IRF-1) is important during the maturation of natural killer 1.1+ T cell receptor-alpha/beta+ (NK1+ T) cells, natural killer cells, and intestinal intraepithelial T cells. J Exp Med 187:967–972.

Su AI, Pezacki JP, Wodicka L, Brideau AD, Supekova L, Thimme R, Wieland S, Jens B, Purcell RH, Schultz PG, Chisari FV. 2002. Genomic analysis of the host response to hepatitis C virus infection. Proc Natl Acad Sci USA 99:15669–15674.

Takaku S, Nakagawa Y, Shimizu M, Norose Y, Maruyama I, Wakita T, Takano T, Kohara M, Takahashi H. 2003. Induction of hepatic injury by hepatitis C virus-specific CD8+ murine cytotoxic T

lymphocytes in transgenic mice expressing the viral structural genes. Biochem Biophys Res Commun 301:330–337.

Tanaka T, Kitamura F, Nagasaka Y, Kuida K, Suwa H, Miyasaka M. 1993. Selective long-term elimination of natural killer cells *in vivo* by an anti-interleukin 2 receptor beta chain monoclonal antibody in mice. J Exp Med 178:1103–1107.

Thimme R, Oldach D, Chang KM, Steiger C, Ray SC, Chisari FV. 2001. Determinants of viral clearance and persistence during acute hepatitis C virus infection. J Exp Med 194:1395–1406.

Thimme R, Bukh J, Spangenberg HC, Wieland S, Pemberton J, Steiger C, Govindarajan S, Purcell RH, Chisari FV. 2002. Viral and immunological determinants of hepatitis C virus clearance, persistence, and disease. Proc Natl Acad Sci USA 99:15661–15668.

Tseng CT, Klimpel GR. 2002. Binding of the hepatitis C virus envelope protein E2 to CD81 inhibits natural killer cell functions. J Exp Med 195:43–49.

Tsukiyama-Kohara K, Tone S, Maruyama I, Inoue K, Katsume A, Nuriya H, Ohmori H, Ohkawa J, Taira K, Hoshikawa Y, Shibasaki F, Reth M, Minatogawa Y, Kohara M. 2004. Activation of the CKI-CDK-Rb-E2F pathway in full genome hepatitis C virus-expressing cells. J Biol Chem 279:14531–14541.

Vidal-Castineira JR, Lopez ZA, Diaz PR, Alonso AR, Martinez BJ, Perez R, Fernandez SJ, Melon S, Prieto J, Rodrigo L, López LC. 2010. Effect of killer immunogloblin-like receptors in the response to combined treatment in patients with chronic hepatitis C virus infection. J Virol 84: 475–481.

Vilasco M, Larrea E, Vitour D, Dabo S, Breiman A, Reqnault B, Riezu JI, Eid P, Prieto J, Meurs EF. 2006. The protein kinase IKKepsilon can inhibit HCV expression independently of IFN and its own expression is downregulated in HCV-infected livers. Hepatology 44:1635–1647.

Wakita T, Taya C, Katsume A, Kato J, Yonekawa H, Kanegae Y, Saito I, Hayashi Y, Koike M, Kohara M. 1998. Efficient conditional transgene expression in hepatitis C virus cDNA transgenic mice mediated by the Cre/loxP system. J Biol Chem 273:9001–9006.

Yoon JC, Shiina M, Ahlenstiel G, Rehermann B. 2008. Natural killer cell function is intact after direct exposure to infectious hepatitis C virions. Hepatology 49:12–21.

JOURNAL OF CLINICAL MICROBIOLOGY, Nov. 2010, p. 3843–3851 Vol. 48, No. 11
0095-1137/10/$12.00 doi:10.1128/JCM.00415-10

Detection of Hepatitis B and C Viruses in Almost All Hepatocytes by Modified PCR-Based *In Situ* Hybridization▽

Hideko Nuriya,[1] Kazuaki Inoue,[1,2] Takeshi Tanaka,[3] Yukiko Hayashi,[4] Tsunekazu Hishima,[4] Nobuaki Funata,[4] Kyosuke Kaji,[5] Seishu Hayashi,[3] Shuichi Kaneko,[5] and Michinori Kohara[1]*

Department of Microbiology and Cell Biology, Tokyo Metropolitan Institute of Medical Science, 2-1-6 Kamikitazawa, Setagaya-ku, Tokyo 156-0057, Japan[1]; Division of Gastroenterology, Showa University Fujigaoka Hospital, 1-30 Aoba-ku, Fujigaoka, Yokohama 227-8501, Japan[2]; Liver Unit, Tokyo Metropolitan Komagome Hospital, 3-18-22 Honkomagome, Bunkyo-ku, Tokyo 113-8613, Japan[3]; Department of Pathology, Tokyo Metropolitan Komagome Hospital, 3-18-22 Honkomagome, Bunkyo-ku, Tokyo 113-8613, Japan[4]; and Department of Gastroenterology, Kanazawa University Graduate School of Medical Science, Ishikawa 920-8641, Japan[5]

Received 28 February 2010/Returned for modification 22 April 2010/Accepted 16 August 2010

Although PCR-based *in situ* hybridization (PCR-ISH) can be used to determine the distribution and localization of pathogens in tissues, this approach is hampered by its low specificity. Therefore, we used a highly specific and sensitive PCR-ISH method to reveal the lobular distribution and intracellular localization of hepatitis B virus (HBV) and HCV in chronic liver disease and to clarify the state of persistent HBV and HCV infection in the liver. HBV genomic DNA was detected in almost all hepatocytes, whereas HBV RNA or protein was differentially distributed only in a subset of the HBV DNA-positive region. Further, HCV genomic RNA was detected in almost all hepatocytes and was localized to the cytoplasm. HCV RNA was also detected in the epithelium of the large bile duct but not in endothelial cells, portal tracts, or sinusoidal lymphocytes. In patients with HBV and HCV coinfection, HCV RNA was localized to the noncancerous tissue, whereas HBV DNA was found only in the cancerous tissue. Using this novel PCR-ISH method, we could visualize the staining pattern of HBV and HCV in liver sections, and we obtained results consistent with those of real-time detection (RTD)-PCR analysis. In conclusion, almost all hepatocytes are infected with HBV or HCV in chronic liver disease; this finding implies that the viruses spreads throughout the liver in the chronic stage.

Hepatitis B virus (HBV) and hepatitis C virus (HCV) are the primary causative agents of chronic liver disease (2, 9, 17). HBV infection remains a global health problem; it is estimated that 350 million individuals are persistently infected with the virus and that approximately 15% to 25% of these individuals will die due to the sequelae of the infection (23, 29). Further, more than 170 million people are infected with HCV worldwide (21). HCV has a single-stranded RNA genome (8, 19), does not have canonical oncogenes, and can easily establish chronic infection without integration into the host genome (3, 20), resulting in hepatic steatosis and hepatocellular carcinoma (HCC) (28). The viruses share a similar route of transmission, such as via the transfusion of infected blood or body fluids or use of contaminated needles.

Several studies have shown that 10% to 35% of the individuals infected with HBV also have HCV infection, although the prevalence varies depending on the population studied (4, 32, 34). The relationship between coinfection and acceleration of malignant transformation remains unclear, but HBV and HCV coinfection seems to alter the natural history of both HBV-related and HCV-related liver disease (2, 12). HCV has been shown to inhibit HBV gene expression (7, 15). The high prevalence of occult HBV infection may indicate that HCV also inhibits HBV replication (34). Most epidemiological studies of HBV have been performed by using diagnostic serological assays (16). We recently used a novel, highly sensitive diagnostic PCR method to demonstrate that the HBV genome is detectable in the sera of a substantial proportion of patients with chronic HCV infection who are seronegative for the standard HBV-related markers (1, 34). Further, we reported the levels of HBV DNA and HCV RNA in cancerous and noncancerous liver tissue using real-time detection (RTD)-PCR (34). RTD-PCR is an accurate assay method, but it can determine the levels of genomic DNA and RNA only in homogenized tissue. In this study, we developed a PCR-based *in situ* hybridization (PCR-ISH) method for detecting and visualizing HBV DNA, HBV RNA, and HCV RNA and comparing their protein expression patterns, with the aim to reveal the lobular distribution and intracellular localization of HBV and HCV in chronic liver disease and to clarify the state of persistent HBV and HCV infection in the liver.

MATERIALS AND METHODS

Patients. Twenty-nine patients were admitted to Tokyo Metropolitan Komagome Hospital for the treatment of hepatic tumors. Of these patients, 14 were considered to have chronic HCV infection (persistently positive results for HCV antibody), 8 were diagnosed with chronic hepatitis B (persistently positive results for HBV surface antigen [HBsAg]), and 7 showed negative results for both viral markers but had metastatic liver cancer (6 with colonic cancer and 1 with gastric cancer). We used four samples from seven patients as controls for PCR-ISH and four samples from seven patients as controls for reverse transcriptase PCR (RT-PCR)–ISH (Table 1). Of the 14 patients with chronic hepatitis C, two showed positive results for HBV DNA by RTD-PCR. HBsAg and second-generation HCV antibody were measured by using enzyme-linked immunosor-

* Corresponding author. Mailing address: Department of Microbiology and Cell Biology, The Tokyo Metropolitan Institute of Medical Science, 2-1-6, Kamikitazawa, Setagaya-ku, Tokyo 156-8506, Japan. Phone: 81-3-5316-3232. Fax: 81-3-5316-3137. E-mail: kohara-mc@igakuken.or.jp.

▽ Published ahead of print on 25 August 2010.

TABLE 1. Patient profiles and results of the present study

Patient no.	Age (yr)	Gender[a]	HCV antibody	HBs Ag	Liver histology	RT-PCR–ISH HCV	PCR-ISH HBV	Serum HBV DNA (copies/ml)[b]	Serum HCV RNA		IFN treatment	Note
									Copies/ml	KIU/ml[d]		
1	53	M	−	+	A2F3		+	1.1×10^2			−	
2	42	M	−	+	A2F2		+	4.0×10^5			−	Fig. 2A
3	43	M	−	+	A2F3		+	1.6×10^7			−	
4	53	M	−	+	A2F4		+	6.4×10^3			−	Fig. 1A
5	55	M	−	+	A2F3		+	1.0×10^3			−	Fig. 3A
6	54	M	−	+	A2F4	−	+	NT[c]			−	
7	31	M	−	+	A3F3		+	3.0×10^9			+	
8	61	F	−	+	A3F3		+	NT			−	
9	63	M	+	−	A3F4	+	−		5.6×10^6		−	Fig. 4D
10	56	M	+	−	A2F3	+	−		NT		+	
11	67	F	+	−	A3F4	−	−		NT		−	
12	73	M	+	−	A2F4	+			1.2×10^6		−	Fig. 1B
13	68	F	+	−	A3F4	+			1.1×10^6		−	
14	76	F	+	−	A2F4	+			9.5×10^5		−	Fig. 4A
15	62	M	+	−	A2F3	+			7.2×10^5		−	
16	65	M	+	−	A3F4	+			NT		−	
17	60	F	+	−	A3F4	+				41	−	
18	48	F	+	−	A2F1	+			7.6×10^6	>850	−	Fig. 4C
19	43	M	+	−	A2F3	+				389	−	
20	59	M	+	−	A2F3	+				>850	−	
21	72	F	+	−	A2F4	+	+	3.9×10^1	5.0×10^7			Fig. 5
22	69	M	+	−	A2F3	+	+	5.0×10^1	3.0×10^7			
23	69	M	−	−	Normal	−	−					Gastric cancer
24	58	M	−	−	Normal		−					Colon cancer
25	58	M	−	−	Normal	−						Colon cancer
26	59	F	−	−	Normal	−						Colon cancer
27	65	M	−	−	Normal	−						Colon cancer
28	47	M	−	−	Normal		−					Colon cancer
29	81	F	−	−	Normal		−					Colon cancer

[a] M, male; F, female.
[b] Serum HBV DNA was positive in patients 21 and 22.
[c] NT, not tested.
[d] KIU, kilo international units.

bent assay (ELISA) kits (Abbott Laboratories, Chicago, IL, and International Reagent Corp., Kobe, Japan, respectively). All 29 patients underwent hepatic resection. Histological evaluation of the liver was carried out according to the METAVIR scoring system (3).

Ethical approval. The Institutional Review Board of Tokyo Metropolitan Komagome Hospital approved the study. Written informed consent was obtained from all the subjects.

Sample preparation. The liver tissue samples for HBV DNA detection were fixed in 10% buffered formalin (pH 7.4) for 18 h, embedded in paraffin, cut into 6-μm-thick sections, and mounted on silane-coated glass slides for use with a GeneAmp *in situ* PCR system 1000 unit (Applied Biosystems, Foster City, CA). The slides were washed thrice in xylene for 8 min at each washing, rinsed thrice in 99.5% ethanol and 75% ethanol for 5 min at each rinsing, and rehydrated in distilled water for deparaffinization. For detecting HBV mRNA and HCV RNA, OCT-embedded frozen liver tissue samples were cut into 10-μm-thick sections and mounted on silane-coated glass slides. They were then fixed in 10% buffered formalin (pH 7.4) for 17 to 21 h, rinsed twice in distilled water treated with 0.01% diethylpyrocarbonate (DEPC) for 2 min at each rinse, rinsed in 99.5% ethanol for 1 min, and then air dried and stored at −80°C until use. The tissue sections on the glass slides were digested with proteinase K (1 to 30 μg/ml and 1 to 200 μg/ml for the noncancerous and cancerous regions of the paraffin-embedded sections, respectively; 0.008 to 1.0 μg/ml for the frozen sections) in 50 mM Tris (pH 7.5) at 37°C for 30 min in a humidified chamber. Subsequently, proteinase K was inactivated at 97°C for 10 min, and then the sections were rinsed with distilled water, dehydrated in 99.5% ethanol, and air dried.

Primers and probes for PCR-ISH and RT-PCR–ISH. The primers used to amplify the S and X regions of HBV and the 5′ untranslated region (5′-UTR) of HCV as well as the corresponding probes are listed in Table 2. We created a digoxigenin (DIG)-dUTP tail at the 3′ end of the 5′-DIG probe using a DNA tailing kit (Roche, Basel, Switzerland).

PCR-ISH for detecting HBV DNA. PCR was performed by using one of two sets of antisense and sense primers complementary to the sequences located in the S and X regions of HBV. The PCR mixture contained 10 mM Tris-HCl (pH 8.3), 50 mM KCl, 3.0 mM $MgCl_2$, 0.8 mM each primer, 197 mM deoxynucleoside triphosphates (dNTPs), and 10 U/50 μl *Taq* DNA polymerase (AmpliTaq Gold; Applied Biosystems).

The tissue slides were warmed to 70°C, and 50 μl of the PCR mixture was overlaid onto the proteinase K-treated tissue specimens. An Ampli cover disc with Ampli cover clips (Applied Biosystems) was attached to each specimen. The slides were placed in the GeneAmp *in situ* PCR system 1000 unit at 70°C. PCR was performed at 95°C for 10 min, followed by 35 to 55 cycles at 95°C for 30 s and 60°C for 2 min and a final extension at 72°C for 10 min. Immediately after the PCR, the slides were fixed in 4% paraformaldehyde in phosphate-buffered saline (PBS) for 10 min at 37°C, washed in 2× SSC (1× SSC is 0.15 M NaCl plus 0.015 M sodium citrate) for 2 min, rinsed with distilled water for 2 min, dehydrated in 99.5% ethanol for 1 min, and then air dried. ISH was performed by mixing the DIG-labeled probe (final concentration, 100 ng/ml) with 65 μl of hybridization buffer (50% deionized formamide, 4× SSC, 1× Denhardt's solution [0.2% bovine serum albumin {BSA}, 0.2% polyvinyl pyrrolidone, 0.2% Ficoll 400], 100 μg/ml denatured salmon sperm DNA, 100 μg/ml yeast RNA, and 1 mM EDTA) and then adding the mixture to each section, heating to 97°C for 10 min, and cooling to 37°C in decrements of 1°C/min (27). Hybridization was carried out overnight at 37°C. Stringency washes were conducted with the following: 2× SSC twice for 10 min at 37°C, 0.03× SSC for 10 min at 50°C, 0.1% Triton X-100 in TBS (0.1 M Tris [pH 7.5], 0.1 M NaCl) for 10 min at room temperature, and TBS for 5 min at room temperature. After incubation in blocking reagent (0.1 M Tris

[pH 7.5], 0.1 M NaCl, 10% sheep serum, 3% BSA) at room temperature for 15 min, the slides were covered with 100 μl anti-DIG antibody conjugated with alkaline phosphatase (Roche) and diluted at 1:900 with 1% BSA in TBS at 37°C for 60 min. After this reaction, the slides were washed twice (3 min each) with 0.1% Triton X-100 in TBS, then with TBS alone, and finally with APS (0.1 M Tris [pH 9.0], 0.1 M NaCl, 50 mM $MgCl_2$) at room temperature. The slides were incubated in 100 μl dye solution (338 μg/ml nitroblue tetrazolium chloride [NBT], 175 μg/ml 5-bromo-4-chloro-3-indolyl-phosphate 4-toluidine salt [BCIP], and 450 μM Levamisole [Vector Labs, Burlingame, CA] in APS) at 37°C in the dark. After sufficient color development, they were washed with deionized water for 1 min and then mounted with aqueous mounting medium.

RT-PCR–ISH for detecting HBV RNA. The OCT-embedded frozen sections were placed on glass slides. After proteinase K treatment, the tissue sections were digested with RNase-free DNase I (Roche; diluted to 3 U/μl in 0.1 M sodium acetate and 5 mM $MgSO_4$). The DNase I reaction mixture (66 μl) was overlaid onto the tissue sections, which were then enclosed in a frame. The slides were reacted in an aluminum box at 37°C for 20 min and inactivated at 97°C for 10 min. They were then washed in DEPC-treated water, dehydrated in 99.5% ethanol, and air dried.

Moloney murine leukemia virus (MMLV) reverse transcriptase (10 U/μl; Invitrogen, Carlsbad, CA) was used in a reaction mixture containing 10 mM Tris-HCl (pH 8.3), 50 mM KCl, 5.0 mM $MgCl_2$, 1 μM antisense primer, 1 mM dNTPs, 2 U/μl RNase inhibitor (Takara, Otsu, Japan), and 10 mM dithiothreitol (DTT). The specimens were then overlaid with the mixture, reacted at 42°C for 60 min, washed with distilled water, dehydrated in 99.5% ethanol, and air dried. The subsequent procedures were the same as described for PCR-ISH.

Immunohistochemical staining for detecting HBV proteins. Deparaffinized formaldehyde-fixed sections or fixed frozen liver tissue sections on glass slides were soaked in distilled water, digested with 0.1% pronase (protease P8038 XXIV; Sigma-Aldrich, Tokyo, Japan) for 1 min, and washed with PBS at room temperature. After 30 min of incubation in blocking reagent (1% BSA and 2.5 mM EDTA in PBS) at room temperature, the slides were reacted with 100 μl of anti-HBs and anti-HBc polyclonal antibody solutions for 3 h at room temperature and then overnight at 4°C. The following polyclonal antibodies were used: anti-HBs rabbit polyclonal antibody anti-HBc rabbit polyclonal antibody (Novocastra Laboratories, Newcastle, United Kingdom), or normal rabbit serum diluted in blocking reagent. After the reaction, the slides were washed four times with PBS at room temperature and incubated for 60 min at room temperature in 100 μl anti-rabbit IgG conjugated with peroxidase (Amersham ECL; GE Healthcare, Piscataway, NJ) diluted to 1:100 in blocking reagent. The slides were then washed four times with PBS at room temperature and stained by using 3,3′-diaminobenzidine tetrahydrochloride (DAB) (Vector Labs). Following counterstaining with Mayer's hematoxylin solution, the tissue specimens were dehydrated in 99.5% ethanol and 80% xylene. The slides were sealed by using Bioleit (Oken Shoji, Tokyo, Japan).

RT-PCR–ISH for detecting HCV RNA. HCV RNA was detected by using methods similar to those used for detecting HBV RNA except for the following steps: the DNase I step was omitted, and 1.5 mM $MgCl_2$ was used in the PCR mixture.

Primers and probe sets in RTD-PCR for quantifying HBV DNA, HCV RNA, β-actin DNA, and GAPDH mRNA. The primer sets to quantify the S and X regions of HBV were the same as those used for PCR-ISH. The TaqMan probes for these regions, the primers and probe designed to quantify the 5′-UTR of HCV (33), and those used to quantify β-actin genomic DNA and GAPDH (glyceraldehyde-3-phosphate dehydrogenase) mRNA (internal control) are shown in Table 2. Each PCR comprised 50 cycles (95°C for 30 s, 60°C for 40 s, and 72°C for 30 s) in a real-time PCR system (ABI Prism 7700 sequence detector system; Applied Biosystems).

Amplicor monitor assays. The Amplicor monitor assays were performed as described previously (22, 24, 33, 36).

HE staining. HBV- or HCV-infected deparaffinized formaldehyde-fixed sections or fixed frozen liver tissue sections were stained with hematoxylin and eosin (HE).

LCM of liver tissue. A frozen liver tissue sample was sectioned by using a cryostat and fixed in acetone, followed by HE staining. Laser capture microdissection (LCM) was performed by using an LM 200 system (Olympus, Tokyo, Japan) as described previously (6, 11). This procedure produced approximately 30 hepatocytes from each of three areas (perivenular, intermediate, and periportal) in the section. Total RNA was extracted from the LCM samples, and HCV RNA and GAPDH mRNA were quantified by RTD-PCR.

TABLE 2. Primers and probes for PCR-ISH and RT-PCR

Technique	Virus or protein (region)	Primer or probe		
		Type	Description, nucleotides	Sequence
PCR-ISH	HBV (HBs)	Primer	Forward (HB-166-S21), 166–186	5′-CACATCAGGATTCCTAGGACC-3′
			Reverse (HB-344-R20), 344–325	5′-AGGTTGGTGAGTGATTGGAG-3′
		Probe	(HB-242-S45D), 242–286	5′-(DIG)-CAGAGTCTAGACTCGTGGTGGACTTCTCTCAATTTTCTAGGGGGA-(DIG)n-3′
	HBV (HBx)	Primer	Forward (HB-1584-S21), 1584–1604	5′-CTTCGCTTCACCTCTGCACGT-3′
			Reverse (HB-1744-R23), 1744–1722	5′-CCCAACTCCTCCCAGTCCTTAAA-3′
		Probe	(HB-1705-R45D), 1705–1661	5′-(DIG)-TATGCCTCAAGGTCGGTCGTTGACATTGCTGAGAGTCCAAGAGTC-(DIG)n-3′
RT-PCR–ISH	HCV (5′-UTR)	Primer	Forward (R6-129-S19), 129–147	5′-CCGGGAGAGCCATAGTGGT-3′
			Reverse (R6-290-R19), 290–272	5′-AGTACCACAAGGCCTTTCG-3′
		Probe	(R6-225-S45D), 225–269	5′-(DIG)-ATTTGGGGCGTGCCCCCGCGAGACTGCTAGCCGAGTAGTGTTGGGT-(DIG)n-3′
TaqMan	HBV (S)	Probe	Forward (HB-242-S26FT), 242–267	5′-CAGAGTCTAGACTCGTGGTGGACTTC-3′
	HBV (X)	Probe	Forward (HB-1681-S25FT), 1681–1705	5′-TGTCAACGACCGACCTTGAGGCATA-3′
	HCV (5′-UTR)	Primer	Forward (R6-130-S17), 130–146	5′-CGGGAGAGCCATAGTGG-3′
			Reverse (R6-200-R19), 200–272	5′-AGTACCACAAGGCCTTTCG-3′
		Probe	Forward (R6-148-S21FT), 148–168	5′-CTGCCGGAACCGGTGAGTACAC-3′
	β-Actin (genomic DNA)	Primer	Forward (β-ACT-1998-S20), 1998–2017	5′-CAGTGTGACATGGTGCATCT-3′
			Reverse (β-ACT-2246-R24), 2246–2223	5′-GTGAGGATCTTCATGAGGTAGTCA-3′
		Probe	Forward (β-ACT-2063-S22FT), 2063–2084	5′-ACGTTGCTATCCAGGCTGTGCT-3′
	GAPDH	Primer	Forward (GAPDH-514-S24), 514–537	5′-TGCACCACCAACTGCTTAGCACCC-3′
			Reverse (GAPDH-837-R24), 837–814	5′-CTTGATGTCATCATATTTGGCAGG-3′
		Probe	Forward (GAPDH-584-S25FT), 584–608	5′-TGACCACAGTCCATGCCATCACTGC-3′

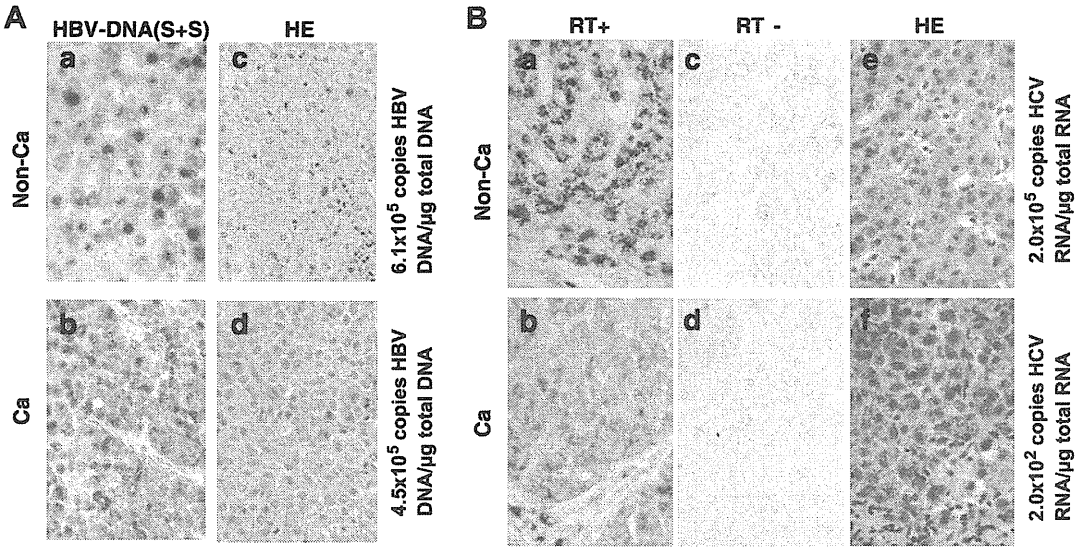

FIG. 1. (A) Panels a and b, HBV DNA detected by PCR-ISH and immunohistochemical staining in noncancerous (Non-Ca) (panel a) and cancerous (Ca) (panel b) liver tissues obtained from a patient infected with HBV. The numbers of PCR cycles were 37 and 42, respectively. Panels c and d, serial sections were stained with HE. Magnification, ×400. S+S, primers and probe targeting the S region of HBV DNA. (B) Panels a and b, HCV RNA detected by RT-PCR–ISH (45 cycles of PCR) in noncancerous (panel a) and cancerous (panel b) tissues obtained from a patient infected with HCV. Panels c and d, no HCV RNA was detected in the RT-negative controls. Panels e and f, serial sections were stained with HE. Magnification, ×400.

RESULTS

Sensitivity and specificity of PCR-ISH versus RTD-PCR for detecting HBV DNA and HCV RNA. PCR-ISH showed positive results for HBV DNA in 10 tissue specimens from eight HBsAg-seropositive patients and two patients whose serum HBV DNA was barely detected by RTD-PCR despite being their HBsAg negative (patients 21 and 22) (Table 1). PCR-ISH yielded negative results for four patients who were negative for serum HBsAg and HCV antibody (patients 23, 24, 28, and 29) and three patients who were negative for serum HBsAg but positive for HCV antibody (patients 9 to 11).

Thirteen of the 14 tissue specimens from the patients with serum HCV antibody had a positive result for HCV RNA by RT-PCR–ISH (sensitivity, 92.9%). In contrast, HCV RNA was not detected by RT-PCR–ISH in four tissue specimens from the patients negative for both HCV antibody and HBsAg (patients 23, 25, 26, and 27) or in the sample from an HBsAg-positive and HCV antibody-negative patient (patient 6).

We performed PCR-ISH and RT-PCR–ISH on the same HBV- or HCV-infected samples from noncancerous and cancerous regions in which we had previously quantitated viral genomic DNA or RNA by RTD-PCR (34). The noncancerous tissue contained 6.1×10^5 copies of HBV DNA/μg total DNA, and the cancerous regions included 4.5×10^5 copies/μg total DNA. Equivalent numbers of cells in the noncancerous and cancerous tissues stained positive for HBV on PCR-ISH (patient 4; Fig. 1A). The PCR-ISH results were consistent with the HBV DNA copy number previously determined by RTD-PCR (34).

Noncancerous tissue from an HCV-positive patient contained 2.0×10^5 copies HCV RNA/μg total RNA, whereas cancerous tissue contained 2.0×10^2 copies/μg total RNA (patient 12; Fig. 1B). HCV RNA was observed by RT-PCR–ISH in hepatocytes of the liver tissue sections from an HCV-infected patient (Fig. 1B). In the noncancerous tissue, an intense hybridization signal was found at the perinuclear sites of almost all the hepatocytes in the section (Fig. 1B, panel a). In contrast, in the cancerous tissue, there was only a weak HCV RNA hybridization signal in the hepatocytes (Fig. 1B, panel b). When the RT step was omitted (control), no HCV RNA was detected in the noncancerous or cancerous tissue sections (Fig. 1B, panels c and d). These results were consistent with the previous quantitation of HCV RNA copy number by RTD-PCR (34).

Detection of HBV DNA by PCR-ISH. HBV DNA was detected by PCR-ISH in the tissue sections obtained from an HBV DNA-seropositive patient. Amplified PCR products were detected by using a probe for either the S or the X region (Fig. 2A, panels a to d) but were not detected by using a heterologous probe (Fig. 2A, panels e and f). Amplification of either the S or the X region of HBV DNA gave the same pattern of hybridization (Fig. 2A, panels a to d). HBV DNA was detected by PCR-ISH in almost all hepatocytes (Fig. 2A, panels a to d) and was very obvious even under low magnification (Fig. 2A, panels a and c). An intense hybridization signal was observed predominantly at the perinuclear site under high magnification (Fig. 2A, panels b and d). In contrast, HBV DNA was not detected by using HBs- and HBx-matched primer and probe combinations in sections obtained from an HBV DNA-seronegative patient (data not shown). DNA fragments amplified by using the S and X region primer sets were 179 bp and 161 bp, respectively (Fig. 2B). Sections from an HBV DNA-seronegative patient were negative in the PCR analysis (data not shown).

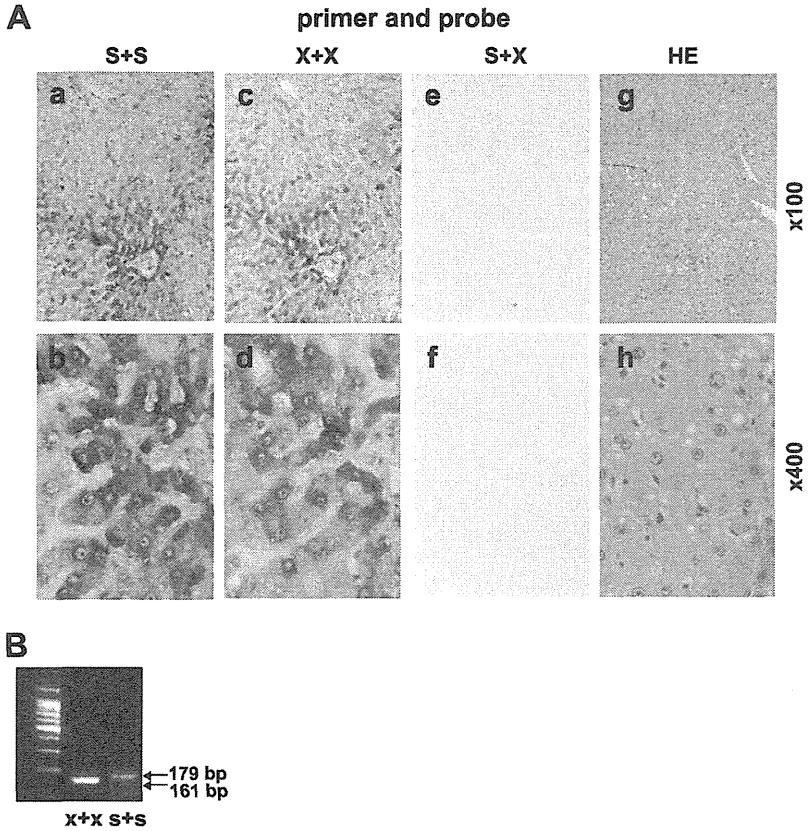

FIG. 2. (A) Panels a to f, HBV DNA detected in liver tissue sections from a patient with chronic hepatitis B by PCR-ISH (42 cycles of PCR). Panels g and h, serial sections were stained with HE. Magnifications, ×100 (panels a, c, e, and g) and ×400 (b, d, f, and h). S+S, primers and probe targeting the S region; X+X, primers and probe targeting the X region; S+X, primers and probe targeting the S and X regions, respectively. (B) Amplified DNA fragments in the PCR mixture of the section in panel A visualized by 3% agarose gel electrophoresis. The PCR product of the X region was 161 bp, and that of the S region was 179 bp.

Localization of HBV DNA, HBV RNA, HBsAg, and HBcAg in liver tissue. HBV DNA, HBV RNA, HBsAg, and HBcAg were detected by PCR-ISH, RT-PCR–ISH, and immunohistochemical staining of serial sections from an HBV-infected patient (patient 5; Fig. 3A, panels a to h). HBV DNA was detected in almost all the hepatocytes by PCR-ISH, although there was wide variation in the hybridization signal intensity between different areas of the section (Fig. 3A, panels a and b). The staining pattern of HBV RNA was similar to that of HBV DNA (Fig. 3A, panels c and d). Intracytoplasmic and intranuclear staining for HBsAg and HBcAg, respectively, was found in some hepatocytes (Fig. 3A, panels f and h). PCR and RT-PCR results were confirmed by gel electrophoresis of the amplified products in the supernatant from the tissue section (Fig. 3B, panels a and b).

Detection of HCV RNA by RT-PCR–ISH. HCV RNA could be detected by RT-PCR–ISH in almost all the hepatocytes in the liver sections obtained from an HCV RNA-seropositive patient (Fig. 4A, panels a and b). Under high magnification, a strong HCV RNA signal was detected in the perinuclear area (Fig. 4A, panel b). A negative-control test (no RT) did not detect any HCV RNA (Fig. 4A, panels c and d). The expected 162-bp DNA fragment amplified by RT-PCR in the supernatant from the tissue section was detected (Fig. 4B, lane 2). In contrast, HCV RNA was not detected in the liver section obtained from an HCV RNA-seronegative patient, regardless of whether RT was used (data not shown).

Isolation of HCV RNA in hepatocytes by LCM. Hepatocyte groups were captured from the perivenular, intermediate, and periportal areas by LCM (Fig. 4C, panel a). HCV RNA was quantified by RTD-PCR in approximately 30 hepatocytes captured by LCM and normalized against the picogram weight of GAPDH mRNA (Fig. 4C, panels b to d); the HCV RNA levels were equivalent in all three regions (Fig. 4C, panel d).

Detection of HCV RNA in the epithelium of the large bile duct. HCV RNA was detected by RT-PCR–ISH in the epithelium of the large bile duct, which was surrounded by dense fibrous and elastic tissue (Fig. 4D, panels a and b). In contrast, no HCV RNA was detected in the epithelium of the small bile duct. Further, HCV RNA was not detected in the portal vein or its branches (Fig. 4D, panel a).

Detection of HBV DNA and HCV RNA in noncancerous and cancerous liver tissue sections obtained from a patient with HBV and HCV coinfection. Figure 5 shows the results for HBV DNA and HCV RNA in liver samples from a patient with HCC having HCV and HBV coinfection. The amounts of serum HBV DNA and HCV RNA were 39 copies/ml and 5×10^7 copies/ml, respectively (patient 21) (34). In the noncancerous

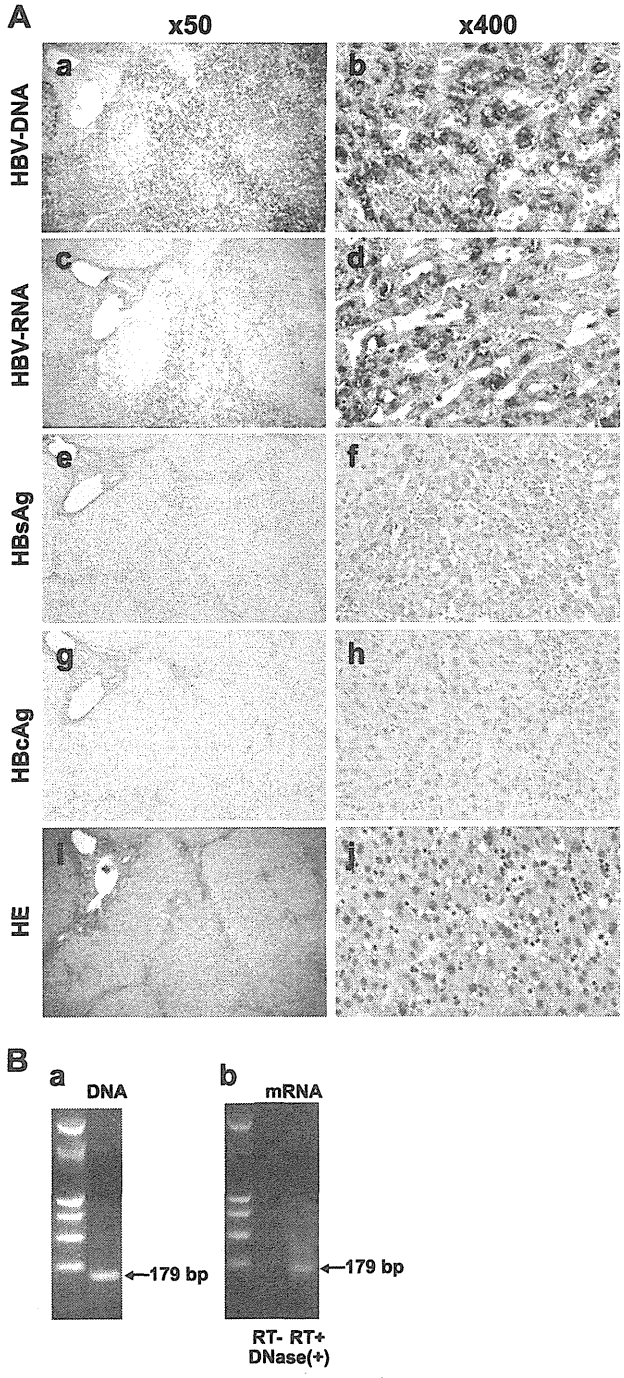

FIG. 3. (A) Panels a to h, HBV DNA, HBV RNA, HBsAg, and HBcAg detected in OCT-embedded frozen liver tissue from a patient with chronic hepatitis B by PCR-ISH (panels a and b), RT-PCR–ISH (panels c and d), and immunohistochemical staining (panels e to h). Panels i and j, HE staining of serial sections. The primers and probe targeted the S region to detect HBV DNA and HBV RNA. Antibodies to the envelope and core proteins were used to detect HBsAg and HbcAg, respectively. Magnifications, ×50 (panels a, c, e, g, and i) and ×400 (panels b, d, f, h, and j). The number of PCR cycles was 42. (B) Amplified DNA fragments in the PCR mixture of the section in panel A. Panel a, the DNA fragments amplified by 42 cycles of PCR were visualized by 3% agarose gel electrophoresis. Panel b, RT-PCR after DNase I treatment (3 U/μl) and negative controls (no RT).

tissue from the patient with HBV and HCV coinfection, there was an intense hybridization signal for HCV RNA on RT-PCR–ISH in almost all the hepatocytes (Fig. 5A, panel b). There was also a positive but weak RT-PCR–ISH signal for HCV RNA in the tumor hepatocytes (Fig. 5B, panel b). Few hepatocytes in the cancerous tissue were positive for HBV DNA by PCR-ISH (Fig. 5B, panel a), and no HBV DNA hybridization signal was detected in the noncancerous tissue (Fig. 5A, panel a).

DISCUSSION

The standard assay for detecting replication of HBV and HCV in tissue is ISH, but results are often inconsistent and sometimes difficult to reproduce. The specificity of ISH is high but its sensitivity low, and it is difficult to detect low copy numbers of the HBV or HCV genome in tissue. PCR technology has been adapted to *in situ* amplification of viral genomes or their replicative intermediates in liver tissue sections, but sensitivity and specificity remain major challenges to the application of this approach (13, 18, 23, 25, 26, 30, 31). Here, we describe the use of a novel, highly specific and sensitive PCR-ISH method to determine the distribution and localization of HBV DNA, HBV RNA, and HCV RNA in both normal and cancerous liver tissues.

PCR-ISH is the most sensitive technology currently available for the detection of viral genomes, but a major potential limitation of this approach is the low specificity. We were able to improve the specificity of PCR-ISH by careful optimization of certain steps. PCR was performed using sets of antisense and sense primers that were complementary to the sequences located in the S and X regions of HBV and the 5′-UTR upstream of the core region of HCV. We added PCR templates to the PCR mixture and then added the PCR mixture to the HBV- or HCV-negative tissue sections. The slides were placed in the GeneAmp *in situ* PCR system 1000 unit, and PCR-ISH was performed as described in Materials and Methods. Following these results, we selected the primer and probe set that did not stain the HBV- or HCV-negative tissue sections by PCR-ISH. Second, the type and concentration of protease and the treatment time were adjusted to optimize permeabilization of membranes and release of protein-nucleic acid cross-linking while avoiding overdigestion. Third, to improve the specificity for detecting viral genomes, we limited the number of PCR cycles and fixed the liver tissue sections in 4% paraformaldehyde immediately after PCR amplification. This step is essential to avoid diffusion of PCR products into neighboring cells, a phenomenon known as the diffusion artifact. Limiting the number of PCR cycles was also important for eliminating the background staining, as too many cycles resulted in high background staining and loss of tissue morphology. Fourth, we added a DIG-dUTP tail at the 3′ ends of the probes for PCR-ISH and RT-PCR–ISH. These 45-mer probes were optimized to improve their sensitivity without impairing the specificity.

HBV DNA was detected by PCR-ISH in a large number of hepatocytes in tissue sections from an HBV DNA-seropositive patient (Fig. 1A, panel a). HBV DNA was also observed by PCR-ISH in tumor hepatocytes in a section of cancerous tissue from the same patient (Fig. 1A, panel b). As shown in Fig. 2A,

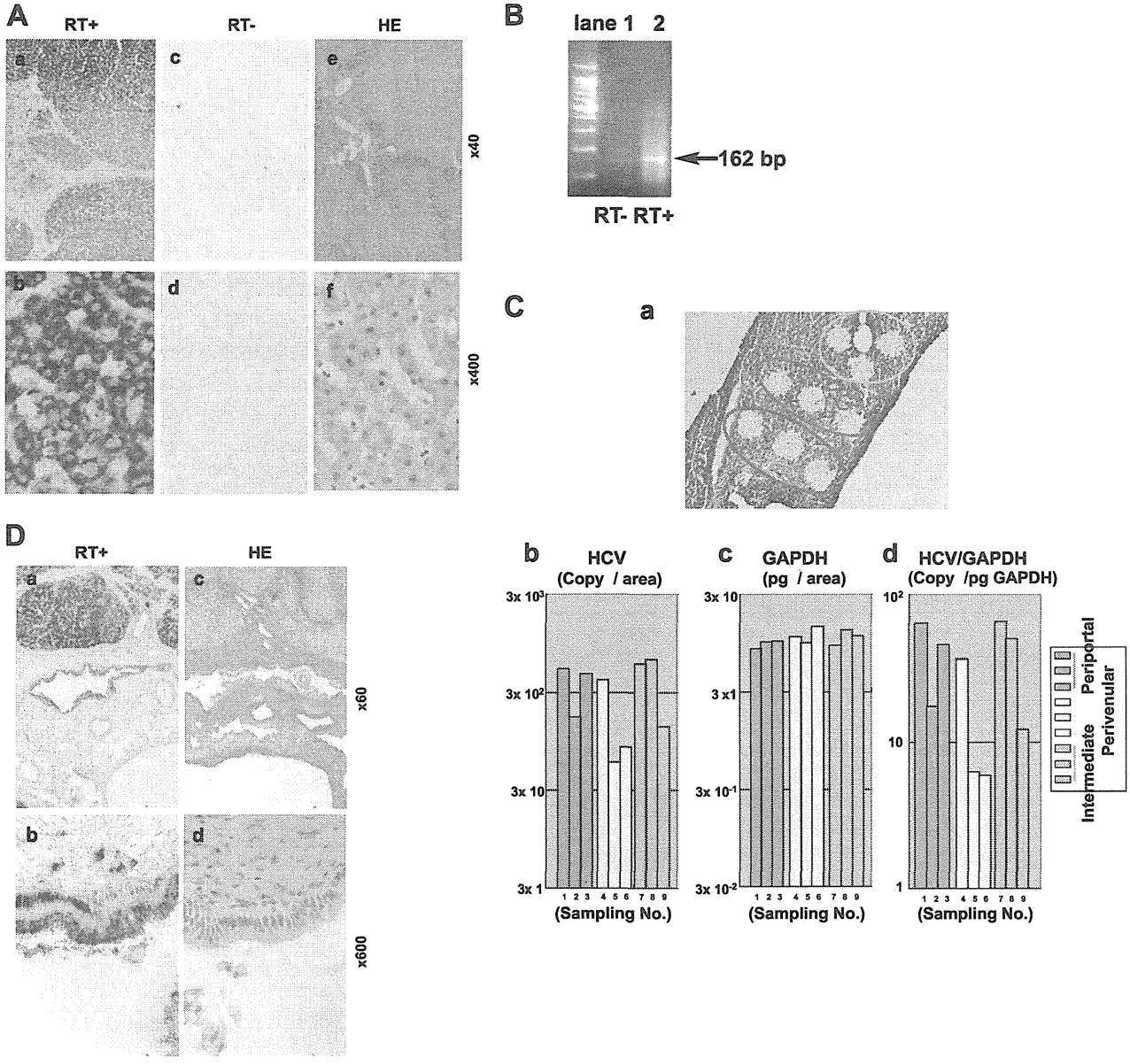

FIG. 4. (A) Panels a and b, HCV RNA detected in liver tissue samples from a patient with chronic hepatitis C by RT-PCR–ISH. Panels c and d, HCV RNA was not detected in a negative control (no RT). The number of PCR cycles was 45. Panels e and f, serial sections were stained with HE. Magnifications, ×40 (panels a, c, and e) and ×400 (panels b, d, and f). (B) DNA fragments in the PCR mixture of the section in panel A were amplified with the RT step and detected by 3% agarose gel electrophoresis. Amplification without the RT step resulted in no detection of DNA fragments. (C) Panel a, after LCM of nine areas, sections of liver tissue obtained from a patient with chronic hepatitis C were stained with HE. Panels b and c, HCV RNA and GAPDH mRNA in each of the areas were quantified by RTD-PCR, and the results are expressed as copy number per LCM area. Panel d, the copy number of HCV RNA was corrected by using the picogram weight of GAPDH. (D) Panels a and b, HCV RNA detected in the epithelium of the large bile duct by RT-PCR–ISH. The number of PCR cycles was 45. Panels c and d, serial sections were stained with HE. Magnifications, ×60 (a and c) and ×600 (b and d).

we obtained clear and reproducible patterns of distribution or localization of the viral genomes in the tissue sections. The visual patterns of HBV DNA distribution were similar, irrespective of the primer sets and probes (Fig. 2A, panels a to d). These data indicate that our technique is highly specific and reproducible for the detection of HBV DNA.

The staining pattern of HBV RNA was similar to that of HBV DNA (Fig. 3A, panels c and d). HBV DNA was also observed by PCR–ISH in tumor hepatocytes in a section of cancerous tissue from an HBV DNA-seropositive patient (Fig. 1A, panel b), but neither HBsAg nor HBcAg was detected in this section (data not shown). As shown in Fig. 3, the intensity of HBV DNA by PCR-ISH was almost the same as that of HBV RNA by RT-PCR–ISH but did not coincide with the